Spectral-admittance and certification theory of multiresonator quantum memories

Maxim Vyacheslavovich Churilov
Independent Researcher, Orenburg, Russian Federation

June 2026

Abstract

Multiresonator quantum memories are commonly analyzed through specific combs, cavity topologies, or echo protocols. This work formulates them instead as passive spectral-admittance synthesizers with controlled storage dilations. In the weak-excitation regime the prompt reflection coefficient is the Cayley transform of a positive-real self-energy generated by resonator and matter degrees of freedom. For a lossless controlled-dilation device, the write defect of a one-photon wavepacket is exactly the prompt reflected spectral power. Hence the worst-case write efficiency on a continuous signal band is $1 - \operatorname{ess\,sup} |r|^2$, and the vector-port generalization is obtained by replacing $|r|$ with the largest singular value of the prompt scattering matrix.

The formulation gives both impossibility results and constructive certificates. A finite time-independent passive one-port realization cannot be exactly reflectionless on a nonzero continuous band: if a rational reflection coefficient vanishes on such an interval, analyticity forces it to vanish identically, whereas every finite resonator realization has $r(s) \to 1$ at high frequency. The associated Bode–Fano area law gives a stronger bandwidth–efficiency ceiling. Conversely, passive minimax matching is a well-posed positive-real approximation problem under explicit linewidth, detuning and oscillator-strength bounds; finite atomic measures are dense, finite-grid continuum certificates have sparse atomic witnesses, and the fixed-pole oscillator-strength subproblem is convex.

The paper turns a spectral matching curve into an operational memory certificate. Finite measurement grids certify a whole band only with a model or derivative margin. Magnitude-only reflection data are insufficient: the complex response must be compatible with a stable Schur function, its inverse Cayley admittance must be positive real, and all-pass phase ambiguity must be controlled. Absorption is memory-grade only when the non-reflected amplitude enters controlled storage ports. For finite alphabets, the write Gram matrix, reciprocal round-trip matrix, noise covariance, entanglement fidelity and diamond-distance bound give a linear quantum-channel certificate.

The stationary bounds also identify the resources that bypass them. A known temporal mode can be captured by a gauge-complete dynamic impedance-matching law, and a K-dimensional known alphabet can be captured exactly with K controlled storage modes and a calibrated vector coupling waveform, subject to the explicit bounded-control leakage certificate developed here. Numerical checks in normalized units $\kappa = 2$ give an eleven-internal-mode passive design with $\max_{|\omega|\le 1} |r(\mathrm{i}\omega)| = 0.069464$, certified worst-case write efficiency 0.995175, reciprocal round-trip probability at least 0.990373, verified imaginary-axis and right-half-plane passivity/Schur margins, data-to-band margins, complex-response uncertainty bounds, robustness tests, capped-control dynamic simulations, thermal-noise conversion and finite-alphabet channel-distance certificates. A convex weight-optimization certificate confirms these synthesized designs are optimal for their pole supports, and an optimal minimax search drives the worst-case reflection systematically toward the Bode–Fano floor: the eleven-internal-mode design is improved to $\max_{|\omega|\le 1} |r| = 0.064112$ (write efficiency 0.995890), each optimized design is certified globally minimax-optimal by three concordant tests (equioscillation, the convex weight-optimum, and an independent global search), the optimum is shown to be minimum-phase and to saturate the area law, and the gap to $e^{-\pi}$ is identified with the vanishing out-of-band log-area, which the certified series closes

root-exponentially (a Gonchar–Rakhmanov–Stahl rate), as conjectured. We give a buildable miniresonator recipe and a fabrication-robust synthesis tolerant of ±1% parameter errors.

1 Introduction and problem statement

Quantum memory for light is a reversible interface between travelling photonic modes and stationary matter degrees of freedom. It is a central primitive for quantum repeaters, optical networking, photonic processing and microwave quantum processors. The mature families of optical memories include electromagnetically induced transparency, Raman memories, controlled reversible inhomogeneous broadening, gradient echo memory, atomic frequency combs and cavity-enhanced photon echo schemes [1, 2, 3]. The multiresonator quantum memory (MR-QM) programme initiated by Moiseev and collaborators attacks a specific bottleneck: a single high-Q resonator enhances the light–matter interaction but ordinarily narrows the working spectral range, whereas many controlled resonators can synthesize a broadband spectral response while keeping high local field enhancement [7, 8, 11, 13, 16].

The literature contains several important partial answers. The original spatial-frequency comb of microresonators gives a Bragg-type impedance condition, $\Delta = \pi\Gamma/2$, for efficient broadband storage in a waveguide-coupled resonator array [7]. A microwave proof-of-principle demonstrated controllable resonator frequencies and impedance-matched storage, with measured room-temperature efficiencies at the level expected for the design losses [8, 9]. Spectral-topological designs showed that a small number of resonant absorbers can reach extremely high calculated spectral efficiency near parameter values where the resonance spectrum restructures [11]. Superconducting multiresonator memories have demonstrated on-demand storage and retrieval of weak microwave pulses and time-bin qubits, and recent RF-SQUID-coupled implementations emphasize dynamically switchable storage and pulse-shape preservation [12, 14]. Integrated designs and resonator arrays with atomic ensembles now give a realistic route to chip-scale broadband memories; this direction is reinforced by preparation-free resonator-array proposals, atomic-ensemble MR-QM theory, high-efficiency impedance-matched rare-earth microcavity memories, and recent network-level benchmarking of multimode high-fidelity memories [13, 15, 16, 18, 19].

A general spectral theory remains missing. Existing results are usually obtained for a particular comb, a particular small topology, a particular optimization functional, or a particular approximation to the atomic ensemble. The following questions remain structurally unresolved.

1. What is the complete frequency-domain object that determines write efficiency and fidelity?
2. Which spectral functions are physically realizable by passive resonators and atomic ensembles?
3. Can a finite passive MR-QM be exactly reflectionless on a continuous signal band?
4. If exact finite-band matching is impossible, what replaces it as the correct universal design principle?
5. How are Bragg, impedance, spectral-dispersion and spectral-topological matching conditions unified?
6. How does one pass from an optimized spectral function to experimentally tunable resonator parameters?
7. How can finite-frequency measurements certify a continuum band rather than only the sampled points?
8. Which measured quantities certify a complete write–store–read quantum channel rather than absorption alone?

This paper gives a direct answer. In the linear weak-excitation regime, a one-port MR-QM is a passive linear quantum system. Its prompt reflection coefficient is a scalar Schur function. Equivalently, it is the Cayley transform of a positive-real internal admittance or self-energy. Memory design is therefore a positive-real spectral approximation problem. This point is simple but decisive: it makes clear what can be exact, what can only be approximate, and what data must be optimized.

The main results are summarized as follows.

- The write process is fully characterized by

$$r(s) = \frac{s - \frac{\kappa-\gamma_c}{2} + \Sigma(s)}{s + \frac{\kappa+\gamma_c}{2} + \Sigma(s)}, \tag{1}$$

  where s is the Laplace frequency, κ is the external waveguide coupling of the common resonator, γ_c its parasitic loss, and Σ is the passive self-energy of the auxiliary resonator–matter network.

- The self-energy is positive real:

$$\operatorname{Re}\Sigma(s) \geq 0, \qquad \operatorname{Re} s > 0. \tag{2}$$

  For diagonal auxiliary resonators loaded by inhomogeneously broadened ensembles,

$$\Sigma(s) = \sum_{m=1}^{M} \frac{|g_m|^2}{s + \gamma_{b,m}/2 + \mathrm{i}\Delta_m + \Phi_m(s)}, \tag{3}$$

  with Φ_m again positive real.

- In the absence of parasitic loss, the write efficiency for a one-photon spectrum $f(\omega)$ is exactly

$$\eta_{\mathrm{w}}[f] = 1 - \int |r(\mathrm{i}\omega + 0)|^2 |f(\omega)|^2 \, \mathrm{d}\omega. \tag{4}$$

  The worst-case efficiency over a band $\mathcal{B}$ is

$$\eta_{\mathrm{w}}^{\min}(\mathcal{B}) = 1 - \operatorname*{ess\,sup}_{\omega\in\mathcal{B}} |r(\mathrm{i}\omega + 0)|^2. \tag{5}$$

- A finite passive time-independent MR-QM cannot have $r(\mathrm{i}\omega + 0) = 0$ on a nonzero continuous interval. Exact continuous-band perfect memory requires an infinite/continuum spectral measure, active or time-dependent matching, or restriction to a finite-dimensional signal subspace.

- Finite devices are nevertheless universal in the physically relevant engineering sense: for any target band and error tolerance, the problem is to synthesize a passive rational positive-real Σ_N that minimizes $\|r_N\|_{L^\infty(\mathcal{B})}$. The minimax value is exactly the worst-case memory error.

- The matching hierarchy

$$\Sigma(s_0) = \frac{\kappa - \gamma_c}{2} - s_0, \qquad \Sigma'(s_0) = -1, \qquad \Sigma^{(q)}(s_0) = 0 \quad (q = 2, \ldots, p) \tag{6}$$

  is the local flat-reflection form of this synthesis problem. It unifies ordinary impedance matching, spectral dispersion compensation and spectral-topological tuning.

The resulting conclusion is deliberately sharper than a design recipe. The universal object is not a particular resonator layout, but the positive-real spectral admittance seen by the waveguide. Any optical, microwave, phononic, magnonic or spin-ensemble implementation that realizes the same admittance has the same write efficiency, up to parasitic loss and retrieval control errors.

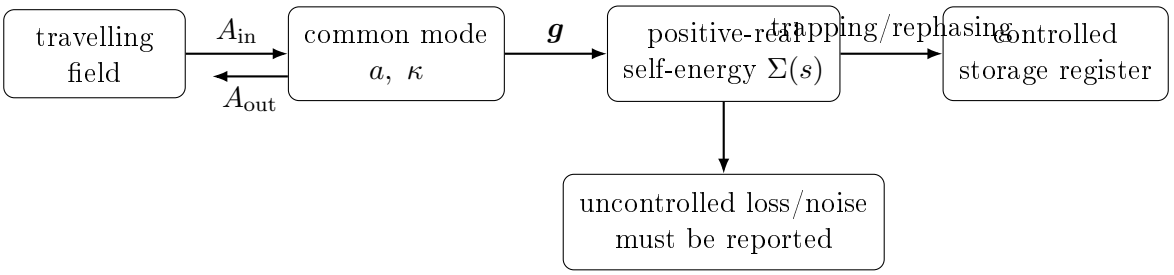

Figure 1: One-port multiresonator memory as a passive spectral-admittance synthesizer. The travelling field sees a common mode loaded by a controlled spectral measure. A memory certificate must identify which absorbed amplitude enters a reversible register and which part enters uncontrolled loss.

2 Assumptions and scope

All results below are formulated in the linear weak-excitation regime. The matter excitations are treated as harmonic bosonic modes, which is the standard single-photon or weak coherent-state approximation to a collectively enhanced ensemble. Saturation, nonlinear photon–photon interactions, control-pulse imperfections during the rephasing stage, and long-time spin decoherence are not hidden inside the spectral-admittance model; they enter as additional loss or noise channels and must be certified separately.

The central object of the theory is the coherent write stage. A high write probability is a quantum-memory probability only when the non-reflected amplitude is mapped into controlled storage degrees of freedom. This is why the paper distinguishes controlled storage ports from uncontrolled dissipative ports and why it gives a noise certificate for occupied environmental modes. The retrieval theorems assume an ideal reciprocal read operation on the stored subspace; deviations from reciprocity are experimentally measurable channel errors, not modifications of the write-admittance theorem.

The scalar one-port theory is the analytically sharp core. Multiport and vector-mode interfaces are included through the prompt scattering matrix $R(\mathrm{i}\omega)$. The corresponding certificate is the largest singular value of R, not a reflection coefficient measured in one selected input polarization or spatial mode. This distinction is essential for comparing broadband memories with different physical encodings.

3 Physical model

3.1 One-port common-resonator architecture

We consider the standard one-port architecture shown schematically in Fig. 1. A travelling field $A_{\mathrm{in}}(t)$ drives a common resonator mode a. The common mode couples to auxiliary resonator modes b_m, and each auxiliary resonator may contain an ensemble of atoms, spins, colour centres, rare-earth ions, quantum dots, or another long-lived matter system. The external waveguide coupling is κ. The intrinsic loss rates of the common and auxiliary resonators are γ_c and $\gamma_{b,m}$. Detunings are measured from the carrier frequency.

In a rotating frame and under the rotating-wave approximation, the linearized Heisenberg–

Langevin equations are

$$\dot{a} = -\frac{\kappa + \gamma_c}{2} a - \mathrm{i} \sum_{m=1}^{M} g_m b_m + \sqrt{\kappa}\, A_{\mathrm{in}} + \sqrt{\gamma_c}\, c_{\mathrm{in}}, \tag{7}$$

$$\dot{b}_m = -\left(\frac{\gamma_{b,m}}{2} + \mathrm{i}\Delta_m \right) b_m - \mathrm{i} g_m^* a - \mathrm{i} \sum_{\alpha} f_{m\alpha} \sigma_{m\alpha} + \sqrt{\gamma_{b,m}}\, d_{m,\mathrm{in}}, \tag{8}$$

$$\dot{\sigma}_{m\alpha} = -\left(\frac{\gamma_{a,m\alpha}}{2} + \mathrm{i}\delta_{m\alpha} \right) \sigma_{m\alpha} - \mathrm{i} f_{m\alpha}^* b_m + \sqrt{\gamma_{a,m\alpha}}\, e_{m\alpha,\mathrm{in}}. \tag{9}$$

Here $\sigma_{m\alpha}$ is the bosonic weak-excitation approximation to the atomic lowering operator of the αth atom or collective spectral class in the mth auxiliary resonator. This approximation is exactly the usual Holstein–Primakoff linearization for a weak signal and an initially unexcited ensemble. The input-output relation is

$$A_{\mathrm{out}}(t) = A_{\mathrm{in}}(t) - \sqrt{\kappa}\, a(t). \tag{10}$$

Different sign conventions replace r by an overall phase; all efficiencies and matching conditions are unchanged.

Let the Laplace transform be $x(s) = \int_0^\infty e^{-st} x(t) \mathrm{d}t$ with $\mathrm{Re}\, s > 0$. Eliminating matter excitations gives

$$\Phi_m(s) = \sum_{\alpha} \frac{|f_{m\alpha}|^2}{s + \gamma_{a,m\alpha}/2 + \mathrm{i}\delta_{m\alpha}}, \tag{11}$$

and

$$b_m(s) = \frac{-\mathrm{i} g_m^* a(s)}{s + \gamma_{b,m}/2 + \mathrm{i}\Delta_m + \Phi_m(s)} + \text{noise terms}. \tag{12}$$

The common mode therefore obeys

$$\left[s + \frac{\kappa + \gamma_c}{2} + \Sigma(s) \right] a(s) = \sqrt{\kappa}\, A_{\mathrm{in}}(s) + \text{noise terms}, \tag{13}$$

with self-energy

$$\boxed{\Sigma(s) = \sum_{m=1}^{M} \frac{|g_m|^2}{s + \gamma_{b,m}/2 + \mathrm{i}\Delta_m + \Phi_m(s)}.} \tag{14}$$

Neglecting noise inputs when computing the coherent scattering amplitude, Eqs. (13) and (10) yield Eq. (1).

3.2 Continuous atomic broadening

For an inhomogeneously broadened ensemble with spectral density $\rho_m(\delta)$ and coupling $f_m(\delta)$,

$$\Phi_m(s) = \int_{\mathbb{R}} \frac{|f_m(\delta)|^2 \rho_m(\delta)}{s + \gamma_a/2 + \mathrm{i}\delta}\, \mathrm{d}\delta. \tag{15}$$

For a Lorentzian profile

$$\rho_m(\delta) = \frac{\Delta_{a,m}/\pi}{\Delta_{a,m}^2 + (\delta - \bar{\delta}_m)^2}, \tag{16}$$

and slowly varying coupling, residue integration gives

$$\Phi_m(s) = \frac{N_m |f_m|^2}{s + \gamma_a/2 + \Delta_{a,m} + \mathrm{i}\bar{\delta}_m}. \tag{17}$$

This is the analytic mechanism behind the effective linewidth broadening used in recent multiresonator ensemble calculations: matter loading changes both the absorptive part and the dispersion of the auxiliary resonator self-energy [16].

3.3 Positive-real property

A scalar function $Y(s)$ is positive real if it is analytic in $\operatorname{Re} s > 0$, real-symmetric, and $\operatorname{Re} Y(s) \geq 0$ for $\operatorname{Re} s > 0$. Positive-real functions are the admittances of passive linear systems.

Lemma 1 (Matter and resonator self-energies are positive real)**.** *Assume $\gamma_{b,m}, \gamma_{a,m\alpha} \geq 0$ and all oscillator strengths are nonnegative. Then $\Phi_m(s)$ and $\Sigma(s)$ are positive real for $\operatorname{Re} s > 0$ whenever the auxiliary resonator network is passive and stable.*

Proof. For Eq. (11),

$$\operatorname{Re} \frac{|f_{m\alpha}|^2}{s + \gamma_{a,m\alpha}/2 + \mathrm{i}\delta_{m\alpha}} = |f_{m\alpha}|^2 \frac{\operatorname{Re} s + \gamma_{a,m\alpha}/2}{|\, s + \gamma_{a,m\alpha}/2 + \mathrm{i}\delta_{m\alpha}\,|^2} \geq 0. \tag{18}$$

The continuous case follows by monotone convergence. A passive interconnection of positive-real one-port admittances is positive real; equivalently, the state-space realization in Eqs. (7)–(9) has a dissipative generator. Thus Eq. (14) is positive real for a stable passive network. In the diagonal form this also follows from the Schur complement of an accretive matrix. □

This lemma is the first key structural point. It says that a multiresonator memory is not an arbitrary spectral filter. It belongs to the positive-real class. Conversely, passive network synthesis says that rational positive-real admittances can be realized by networks of harmonic modes and lossless couplers; in quantum optics this is the passive linear quantum realization theorem [25, 26, 27].

3.4 Schur–positive-real equivalence

The reflection function and the self-energy contain the same information, but in two different analytic classes. The former is a Schur function; the latter is positive real. This equivalence is the inverse-design map.

Theorem 1 (Schur–positive-real memory correspondence)**.** *Assume a lossless one-port memory with $\gamma_c = 0$ and $\kappa > 0$. If Σ is stable and positive real, then*

$$r(s) = \frac{s - \kappa/2 + \Sigma(s)}{s + \kappa/2 + \Sigma(s)} \tag{19}$$

is analytic and contractive in the right half-plane:

$$|r(s)| \leq 1, \qquad \operatorname{Re} s > 0. \tag{20}$$

Conversely, let r be analytic in $\operatorname{Re} s > 0$, let $1 - r(s)$ have no zero there, and define

$$\Sigma_r(s) = \frac{\frac{\kappa}{2}[1 + r(s)] - s[1 - r(s)]}{1 - r(s)}. \tag{21}$$

Then r is realizable by a passive MR-QM of the present one-port form if and only if Σ_r is positive real and belongs to the chosen finite or continuum resonator–matter realization class.

Proof. Let $\operatorname{Re} s > 0$ and write $A(s) = s + \Sigma(s)$. Since $\operatorname{Re} \Sigma(s) \geq 0$, $\operatorname{Re} A(s) > 0$. The Möbius transformation

$$z \mapsto \frac{z - \kappa/2}{z + \kappa/2} \tag{22}$$

maps the right half-plane into the unit disk; hence $|r(s)| \leq 1$. Solving the preceding equation for Σ gives Eq. (21). The converse is therefore immediate: if Eq. (21) is positive real and has a passive realization in the allowed class, substituting it back gives the prescribed r and a passive one-port memory. If Σ_r fails positivity, the target Schur function is a passive filter but not a memory of the specified resonator–matter admittance type. □

This theorem is useful because optimization can be stated either as positive-real approximation of the ideal load or as Schur approximation of the zero-reflection target. The positivity of Eq. (21) is the hidden constraint that distinguishes physically writable memories from arbitrary reflection filters.

3.5 Controlled-storage dilation

A positive-real pole may represent uncontrolled dissipation, but in a memory it must represent a controllable storage channel. The distinction is not semantic: it is the difference between absorption loss and quantum memory. The following elementary dilation is the operational form used throughout the numerical checks.

Theorem 2 (Controlled-storage dilation of a positive-real atom)**.** *Let*

$$\Sigma_N(s) = \sum_{n=1}^{N} \frac{w_n}{s + \Gamma_n + \mathrm{i}\nu_n}, \qquad w_n > 0, \quad \Gamma_n > 0, \tag{23}$$

and consider the one-port common resonator coupled to auxiliary modes b_n with $g_n = \sqrt{w_n}$. Replace the decay Γ_n of each b_n by a one-sided controlled storage port C_n,

$$\dot{b}_n = -(\Gamma_n + \mathrm{i}\nu_n)b_n - \mathrm{i}g_n a - \sqrt{2\Gamma_n}\, C_{n,\mathrm{in}}, \tag{24}$$

$$C_{n,\mathrm{out}} = C_{n,\mathrm{in}} + \sqrt{2\Gamma_n}\, b_n. \tag{25}$$

With all $C_{n,\mathrm{in}}$ in the vacuum, the coherent reflection coefficient in the signal port is exactly the Cayley transform with self-energy Σ_N. Moreover, on the real frequency axis the full scattering matrix from the signal port and all storage ports is unitary, and therefore

$$|r(\mathrm{i}\omega)|^2 + \sum_{n=1}^{N} |t_n(\mathrm{i}\omega)|^2 = 1, \tag{26}$$

where t_n is the transfer amplitude into $C_{n,\mathrm{out}}$. Consequently, for every normalized one-photon wavepacket f,

$$\eta_{\mathrm{store}}[f] = \sum_n \int |t_n(\mathrm{i}\omega)|^2 |f(\omega)|^2 \, \mathrm{d}\omega = 1 - \int |r(\mathrm{i}\omega)|^2 |f(\omega)|^2 \, \mathrm{d}\omega. \tag{27}$$

Proof. Eliminating the auxiliary modes gives

$$b_n(s) = \frac{-\mathrm{i}g_n a(s) - \sqrt{2\Gamma_n} C_{n,\mathrm{in}}(s)}{s + \Gamma_n + \mathrm{i}\nu_n}, \tag{28}$$

hence the coefficient multiplying $a(s)$ in the reduced common-mode equation is $\Sigma_N(s)$. This proves the reflection formula when the storage inputs are vacuum. The enlarged model is a passive Markovian input–output system with Hermitian Hamiltonian and coupling operators $\sqrt{\kappa}\, a$ and $\sqrt{2\Gamma_n}\, b_n$; its transfer matrix is unitary on the imaginary axis. Setting the storage inputs to vacuum and taking the first column of that unitary matrix gives Eq. (26). Integrating Eq. (26) against $|f(\omega)|^2$ gives Eq. (27). □

Thus the linewidths Γ_n in a memory-grade positive-real model must be read as rates into addressable dark spin-wave or rephasing reservoirs, not as uncontrolled heat baths. The theorem is a write-scattering dilation: it proves that the non-reflected probability enters specified controlled channels. It does not by itself prove long-lived, on-demand retrieval from those channels. A complete memory claim must additionally specify the trapping, rephasing, decoupling, or time-reversal operation that maps the outgoing storage-port wavepacket to a stationary mode and

back to the signal port. If a particular experiment cannot reverse, freeze, or rephase those ports, Eq. (27) remains an absorption calculation but not a quantum-memory efficiency. This gives a simple experimental falsifiability criterion for any proposed MR-QM: identify the physical storage ports corresponding to the positive-real atoms of $\Sigma(s)$ and report their retrieval map.

Theorem 3 (Port-to-register criterion)**.** *Let $\mathcal{S} = \mathrm{span}\{f_1, \ldots, f_K\}$ be a finite signal alphabet and let*

$$T : \mathcal{S} \to \mathcal{H}_{\mathrm{port}}$$

be the coherent write map from the input alphabet into the controlled storage-port wavepackets of Theorem 2. Define the write Gram matrix $G = T^\dagger T$. A noiseless register trap that preserves all quantum coherences on the successfully written subspace exists if and only if G has no zero eigenvalue on the subspace to be preserved. In that case there is an isometry $C : \overline{\mathrm{Ran}\, T} \to \mathcal{H}_{\mathrm{reg}}$ such that the trapped register map is CT, with the same Gram matrix G. If $G = I_K$, CT is an isometry on the whole alphabet. If $0 < G < I$, the singular values of CT give the unavoidable mode-dependent write probabilities unless an additional heralding or error-filtering operation is introduced.

Proof. This is the polar decomposition of the write map. Write $T = V(G)^{1/2}$, where V is a partial isometry from the support of G onto $\overline{\mathrm{Ran}\, T}$. A lossless trap is precisely an isometric embedding C of that range into stationary register modes. Then $(CT)^\dagger(CT) = T^\dagger T = G$. If $G = I_K$, the map preserves inner products and is a unitary encoding of the alphabet into the register. If G has a null vector, the corresponding coherent superposition is never written into the controlled ports and no later register operation can reconstruct it without an additional copy of the lost field. □

This criterion is the missing logical bridge between a measured absorption spectrum and a memory claim. The spectral theorem certifies $T^\dagger T$; the experimental protocol must still implement the isometry C and the reciprocal read map. The distinction is especially important for positive-real fits in which part of $\Sigma(s)$ is an actual long-lived register and part is ordinary irreversible damping.

Theorem 4 (Loss-separation identity)**.** *Suppose the same one-port memory also has uncontrolled Markovian loss channels L_q with transfer amplitudes $\ell_q(s)$, in addition to controlled storage-port amplitudes $t_n(s)$. On the imaginary axis the enlarged scattering matrix gives*

$$|r(\mathrm{i}\omega)|^2 + \sum_n |t_n(\mathrm{i}\omega)|^2 + \sum_q |\ell_q(\mathrm{i}\omega)|^2 = 1. \tag{29}$$

Therefore a normalized input spectrum f is stored with probability

$$\eta_{\mathrm{store}}[f] = 1 - \int |r(\mathrm{i}\omega)|^2 |f(\omega)|^2 \, \mathrm{d}\omega - \int \sum_q |\ell_q(\mathrm{i}\omega)|^2 |f(\omega)|^2 \, \mathrm{d}\omega. \tag{30}$$

Proof. Equation (29) is the first-column norm identity for the unitary scattering matrix of the signal, storage and uncontrolled-loss ports. Multiplying by $|f(\omega)|^2$ and integrating gives Eq. (30). □

This identity is the operational distinction between high absorption and high quantum-memory efficiency. A spectrum can be impedance matched and still fail as a quantum memory if most of the non-reflected amplitude exits through uncontrolled loss ports.

4 Storage efficiency as spectral reflection defect

4.1 Single-photon signal space

Let

$$|1_f\rangle = \int_{\mathbb{R}} f(\omega) A_{\mathrm{in}}^{\dagger}(\omega)|\mathrm{vac}\rangle \, \mathrm{d}\omega, \qquad \int |f(\omega)|^2 \, \mathrm{d}\omega = 1 \tag{31}$$

be an incoming one-photon wavepacket. A signal band is a measurable set $\mathcal{B} \subset \mathbb{R}$, and the band-limited single-photon subspace is

$$\mathcal{H}_{\mathcal{B}} = \left\{ f \in L^2(\mathbb{R}) : \operatorname{supp} f \subset \mathcal{B} \right\}. \tag{32}$$

We define write efficiency at the end of the absorption interval as the probability that the excitation is in the controlled memory degrees of freedom rather than in the prompt output or uncontrolled loss channels. In a lossless passive device these are the only two alternatives.

Theorem 5 (Exact write-efficiency identity)**.** *For a stable, lossless, one-port passive MR-QM in the weak-excitation regime,*

$$\eta_{\mathrm{w}}[f] = 1 - \int_{\mathbb{R}} |r(\mathrm{i}\omega + 0)|^2 |f(\omega)|^2 \, \mathrm{d}\omega. \tag{33}$$

Consequently the worst-case write efficiency on a band $\mathcal{B}$ is

$$\eta_{\mathrm{w}}^{\min}(\mathcal{B}) = 1 - \operatorname*{ess\,sup}_{\omega \in \mathcal{B}} |r(\mathrm{i}\omega + 0)|^2. \tag{34}$$

With parasitic loss channels $\ell_j(\omega)$, the identity becomes

$$\eta_{\mathrm{w}}[f] = 1 - \int \left(|r(\mathrm{i}\omega + 0)|^2 + \sum_j |\ell_j(\mathrm{i}\omega + 0)|^2 \right) |f(\omega)|^2 \, \mathrm{d}\omega. \tag{35}$$

Proof. The full field plus internal oscillator evolution generated by Eqs. (7)–(9) is unitary when all loss channels are included as input-output fields. For each frequency, the linear input-output map is a unitary scattering matrix from the incoming waveguide channel to the outgoing waveguide, controlled memory modes and environmental channels. In the one-port lossless case this gives

$$|r(\mathrm{i}\omega + 0)|^2 + \|w(\omega)\|^2 = 1, \tag{36}$$

where $w(\omega)$ is the frequency-domain transfer vector into controlled memory modes at the chosen write time. Parseval's theorem applied to the one-photon spectral amplitude gives Eq. (33). Including environmental channels gives

$$|r|^2 + \sum_j |\ell_j|^2 + \|w\|^2 = 1, \tag{37}$$

and hence Eq. (35). The worst-case formula (34) follows because multiplication by $|r|^2$ on $L^2(\mathcal{B})$ has operator norm $\operatorname{ess\,sup}_{\mathcal{B}} |r|^2$. □

This theorem is the operational reduction of the write problem. A memory paper may report an echo efficiency, a cavity linewidth, an optical depth, or a comb finesse, but the write part of the universal interface is completely determined by $r(\omega)$, uncontrolled loss, and an explicit identification of the controlled storage channels. Retrieval requires the additional inverse map described in Sec. 13, not merely the disappearance of prompt reflection.

4.2 Perfect memory criterion

Corollary 1 (Perfect stationary write criterion)**.** *A lossless one-port passive MR-QM writes every photon in $\mathcal{H}_{\mathcal{B}}$ with unit efficiency if and only if*

$$r(\mathrm{i}\omega + 0) = 0 \quad \text{for almost every } \omega \in \mathcal{B}. \tag{38}$$

For a finite-dimensional stationary signal subspace $\mathcal{S} = \operatorname{span}\{f_1, \dots, f_K\} \subset L^2(\mathbb{R})$, perfect write is equivalent to

$$|r(\mathrm{i}\omega + 0)|\, f(\omega) = 0 \quad \text{for every } f \in \mathcal{S} \text{ and almost every } \omega. \tag{39}$$

Equivalently, after diagonalizing the positive multiplication form on $\mathcal{S}$, all nonzero eigenvectors must be supported inside the zero set of r.

For a nonzero rational r, the boundary zero set on the real-frequency axis is finite unless r vanishes identically. Hence a finite time-independent passive rational device cannot perfectly write any nonzero square-integrable wavepacket whose spectrum occupies a set of positive measure. Exact stationary interpolation is possible only for idealized monochromatic frequency-bin distributions or for non-rational/continuum limits. Exact capture of genuine temporal wavepackets is instead a dynamic-control statement, treated in Theorem 12 and Theorem 13. The finite-alphabet Gram certificate below is therefore an exact efficiency certificate, not a hidden proof of stationary perfect storage for ordinary L^2 pulse modes.

5 Vector-port and multimode prompt-scattering certificate

Many practical interfaces have more than one prompt optical or microwave channel: polarization, counterpropagating modes, spatial modes, frequency bins, or deliberately engineered multiport couplers. The scalar reflection theorem has an immediate operator-valued extension.

Let the incoming signal on a band $\mathcal{B}$ be a vector-valued spectrum

$$f(\omega) \in \mathbb{C}^p, \qquad \|f\|^2 = \int_{\mathcal{B}} \|f(\omega)\|_{\mathbb{C}^p}^2 \, \mathrm{d}\omega = 1.$$

Let $R(\mathrm{i}\omega) \in \mathbb{C}^{p\times p}$ be the coherent prompt scattering matrix from the signal input channels back to the signal output channels after all controlled storage ports have been eliminated.

Theorem 6 (Vector-port storage certificate)**.** *For a lossless controlled-dilation multiresonator memory,*

$$\eta_{\mathrm{w}}[f] = 1 - \int_{\mathcal{B}} f(\omega)^\dagger R(\mathrm{i}\omega)^\dagger R(\mathrm{i}\omega) f(\omega) \, \mathrm{d}\omega. \tag{40}$$

Hence the worst-case write efficiency over all normalized vector wavepackets supported in $\mathcal{B}$ is

$$\eta_{\mathrm{w}}^{\min}(\mathcal{B}) = 1 - \operatorname*{ess\,sup}_{\omega\in\mathcal{B}} \sigma_{\max}(R(\mathrm{i}\omega))^2 . \tag{41}$$

For a finite vector-valued alphabet $f_1, \dots, f_K$, the exact write Gram matrix is

$$G_{ij} = \delta_{ij} - \int_{\mathcal{B}} f_i(\omega)^\dagger R(\mathrm{i}\omega)^\dagger R(\mathrm{i}\omega) f_j(\omega) \, \mathrm{d}\omega. \tag{42}$$

Proof. At each real frequency the enlarged scattering matrix of the prompt channels, controlled storage ports, and any explicitly retained reversible auxiliary ports is unitary. Taking the block column corresponding to the p signal inputs gives

$$R^\dagger R + T^\dagger T = I_p,$$

where T is the transfer matrix into controlled storage ports. Multiplication by $f(\omega)$, integration over the band, and normalization give Eq. (40). The worst-case value of the quadratic form

$$\int f^\dagger R^\dagger R f \, \mathrm{d}\omega$$

over unit vectors in $L^2(\mathcal{B};\mathbb{C}^p)$ is the essential supremum of the largest eigenvalue of $R^\dagger R$, which is $\operatorname{ess\,sup} \sigma_{\max}(R)^2$. Restricting the same quadratic form to a finite orthonormal alphabet gives Eq. (42). □

The one-port formula used below is the special case $p = 1$. The vector theorem is operationally important: a device can have small reflection in one polarization or direction but still fail as a universal interface if $\sigma_{\max}(R)$ is large in another prompt channel. Conversely, a deliberately multiport design should be certified by the singular-value envelope of R, not by one selected scalar reflection trace.

6 Data-to-band certification from finite measurements

Equations (34) and (41) are continuum statements. They are not certified by plotting a finite set of frequency samples unless a rational model, a passivity-constrained fit, or a derivative margin is also reported. This point is operationally important: a narrow under-sampled reflection spike can dominate the worst-case memory error even when all measured points look impedance matched.

Theorem 7 (Finite-sampling storage certificate)**.** *Let $\mathcal{B} = [\omega_-, \omega_+]$, let $\Omega_L = \{\omega_\ell\}_{\ell=1}^L \subset \mathcal{B}$, and define the fill distance*

$$h = \sup_{\omega\in\mathcal{B}} \min_{\ell} |\omega - \omega_\ell|. \tag{43}$$

If the scalar reflection coefficient is C^1 on $\mathcal{B}$ and

$$L_r = \sup_{\omega\in\mathcal{B}} \left| \frac{\mathrm{d}}{\mathrm{d}\omega} r(\mathrm{i}\omega) \right| < \infty, \tag{44}$$

then

$$\operatorname*{ess\,sup}_{\omega\in\mathcal{B}} |r(\mathrm{i}\omega)| \le \rho_{\mathrm{grid}} + L_r h, \qquad \rho_{\mathrm{grid}} = \max_{\ell} |r(\mathrm{i}\omega_\ell)|. \tag{45}$$

Consequently every band-limited one-photon mode satisfies

$$\eta_{\mathrm{w}}[f] \ge 1 - (\rho_{\mathrm{grid}} + L_r h)^2. \tag{46}$$

For a vector interface with prompt matrix $R(\mathrm{i}\omega)$, the same statement holds with

$$\rho_{\mathrm{grid}} = \max_{\ell} \sigma_{\max} R(\mathrm{i}\omega_\ell), \qquad L_R = \sup_{\omega\in\mathcal{B}} \left\| \frac{\mathrm{d}}{\mathrm{d}\omega} R(\mathrm{i}\omega) \right\|_{\mathrm{op}},$$

and L_r replaced by L_R.

Proof. For every $\omega \in \mathcal{B}$, choose a nearest sample ω_ℓ. The fundamental theorem of calculus gives

$$|r(\mathrm{i}\omega) - r(\mathrm{i}\omega_\ell)| \le L_r |\omega - \omega_\ell| \le L_r h,$$

and Eq. (45) follows from the triangle inequality. For matrices, Weyl's singular-value inequality gives

$$\sigma_{\max} R(\mathrm{i}\omega) \le \sigma_{\max} R(\mathrm{i}\omega_\ell) + \|R(\mathrm{i}\omega) - R(\mathrm{i}\omega_\ell)\|_{\mathrm{op}} \le \rho_{\mathrm{grid}} + L_R h.$$

The efficiency statements are Theorems 5 and 6. □

The derivative margin can be obtained analytically from a fitted passive rational model, by interval arithmetic on the fitted transfer function, or conservatively from a dense calibrated scan. Without such a margin a finite plot is a diagnostic, not a certificate. In the numerical section the eleven-mode design is checked both by dense continuum evaluation and by the derivative-aware finite-grid bound (46).

7 Complex-response and causal-realizability certification

A memory certificate cannot be based on a magnitude plot alone. The reflection data must be compatible with a causal passive device and must determine the phase convention used by the write–read channel.

Theorem 8 (Schur–admittance realizability test)**.** *Let $r(s)$ be a scalar rational function analytic in the open right half-plane and let $r(s) \neq 1$ there. In the normalized lossless one-port convention $\kappa = 2$, the only self-energy compatible with r is*

$$\Sigma_r(s) = \frac{1 + r(s)}{1 - r(s)} - s. \tag{47}$$

A necessary condition for passive MR-QM realizability is that Σ_r is positive real,

$$\operatorname{Re} \Sigma_r(s) \geq 0 \qquad (\operatorname{Re} s > 0), \tag{48}$$

and has no unstable pole. Conversely, if a rational Σ is strictly proper, stable and positive real, then

$$r_\Sigma(s) = \frac{s - 1 + \Sigma(s)}{s + 1 + \Sigma(s)} \tag{49}$$

is a stable Schur reflection coefficient, $|r_\Sigma(\mathrm{i}\omega)| \leq 1$ on the frequency axis. If the partial-fraction residues of Σ are positive semidefinite in a passive oscillator realization, Eq. (49) is realized by a finite controlled-dilation MR-QM.

Proof. Solving Eq. (49) for Σ gives Eq. (47). A passive internal network has a positive-real driving-point admittance; hence Eq. (48) and stability are necessary. Conversely, for $\operatorname{Re} s > 0$ write $z = s + \Sigma(s)$. Since $\operatorname{Re} z = \operatorname{Re} s + \operatorname{Re} \Sigma(s) > 0$,

$$\left| \frac{z - 1}{z + 1} \right|^2 = \frac{|z|^2 - 2 \operatorname{Re} z + 1}{|z|^2 + 2 \operatorname{Re} z + 1} \leq 1,$$

which proves Schur contractivity on the boundary by continuity. The final realization statement is the passive-realization lemma applied to the positive-real self-energy; the oscillator-residue condition is precisely the MR-QM subclass of such passive realizations. □

Proposition 1 (Magnitude-only ambiguity)**.** *Let $r(s)$ be any stable Schur reflection coefficient and let $a > 0$. The Blaschke factor*

$$B_a(s) = \frac{s - a}{s + a} \tag{50}$$

is stable and all-pass on the frequency axis: $|B_a(\mathrm{i}\omega)| = 1$. Therefore $\widetilde{r}(s) = B_a(s) r(s)$ has exactly the same reflection magnitude and the same band write-efficiency bound as r, but its phase is shifted by

$$\arg B_a(\mathrm{i}\omega) = \pi - 2 \arctan(\omega / a) \tag{51}$$

up to branch convention, with group-delay contribution

$$\tau_a(\omega) = -\frac{\mathrm{d}}{\mathrm{d}\omega} \arg B_a(\mathrm{i}\omega) = \frac{2a}{a^2 + \omega^2}. \tag{52}$$

Thus magnitude data alone cannot certify temporal-mode preservation, reciprocal readout phase, or causal realizability within a declared memory architecture.

Proof. The pole of B_a is at $-a$, so the factor is stable, and for $s = \mathrm{i}\omega$ the numerator and denominator have the same modulus. The phase and group-delay formulas follow by differentiating the boundary value. Multiplication by B_a leaves $|r|$ unchanged but changes the causal impulse response and the phase of the written mode. A quantum memory certificate must therefore report complex scattering data or an equivalent passive state-space model, not only $|r|$. □

Proposition 2 (Minimum-phase phase recovery and all-pass obstruction)**.** *Let $r(s)$ be a rational stable Schur reflection coefficient with no pole or zero on the imaginary axis. Its boundary magnitude determines only its outer, or minimum-phase, factor. More explicitly,*

$$r(s) = e^{\mathrm{i}\theta} B(s) r_{\mathrm{out}}(s), \tag{53}$$

where B is a finite product of right-half-plane Blaschke factors and $|B(\mathrm{i}\omega)| = 1$. If $B = 1$, the boundary phase of r is fixed, up to the constant θ, by the Hilbert transform of $\log|r(\mathrm{i}\omega)|$. If $B \neq 1$, $|r|$ is unchanged but the group delay and the temporal readout mode change.

Proof. This is the rational right-half-plane inner–outer factorization. The zeros of r in the open right half-plane generate stable all-pass Blaschke factors of the form $(s-a)/(s+\bar{a})$, which have unit modulus on $s = \mathrm{i}\omega$. After removing these factors the remaining zero-free stable factor has an analytic logarithm in the right half-plane. The real boundary value of this logarithm is $\log|r|$, and the harmonic conjugate gives the phase by the Hilbert transform, up to an additive constant. Hence magnitude fixes phase only after the all-pass content has been independently excluded. □

Theorem 9 (Complex-response uncertainty certificate)**.** *Let $R : \mathcal{S} \to L^2(\mathcal{B})$ and $\widehat{R} : \mathcal{S} \to L^2(\mathcal{B})$ be the true and fitted prompt scattering maps on a declared finite alphabet $\mathcal{S}$. Define the write Gram matrices by the full prompt-output norm,*

$$G = I - R^\dagger R, \qquad \widehat{G} = I - \widehat{R}^\dagger \widehat{R}.$$

If

$$\|R - \widehat{R}\|_{\mathcal{S}\to L^2(\mathcal{B})} \le \epsilon, \qquad \|\widehat{R}\|_{\mathcal{S}\to L^2(\mathcal{B})} \le \widehat{\rho}, \tag{54}$$

then

$$\|G - \widehat{G}\| \le \epsilon(2\widehat{\rho} + \epsilon), \tag{55}$$

and therefore

$$\lambda_{\min}(G) \ge \lambda_{\min}(\widehat{G}) - \epsilon(2\widehat{\rho} + \epsilon). \tag{56}$$

For a scalar one-port model acting by multiplication with $r(\mathrm{i}\omega)$ and an orthonormal alphabet $f_1, \dots, f_K$,

$$\widehat{G}_{ij} = \delta_{ij} - \int_{\mathcal{B}} |\widehat{r}(\mathrm{i}\omega)|^2 f_i^*(\omega) f_j(\omega)\, \mathrm{d}\omega. \tag{57}$$

The compressed matrix $\int f_i^* \widehat{r} f_j \,\mathrm{d}\omega$ is a same-alphabet coherent-leakage diagnostic; it must not replace Eq. (57) in a write-efficiency certificate, because prompt photons scattered into modes outside the chosen alphabet are still lost from the memory. The sufficient pointwise condition

$$\operatorname*{ess\,sup}_{\omega\in\mathcal{B}} |r(\mathrm{i}\omega) - \widehat{r}(\mathrm{i}\omega)| \le \epsilon \tag{58}$$

implies the operator hypothesis on every subspace of $L^2(\mathcal{B})$. If the complex error is measured on a finite grid, the same derivative-margin argument as in Theorem 7 gives

$$\epsilon \le \epsilon_{\mathrm{grid}} + L_{\delta r} h.$$

Thus calibrated amplitude and phase errors propagate directly into the finite-alphabet write and reciprocal-readout certificates without hiding out-of-alphabet prompt leakage.

Proof. Write $\Delta = R - \widehat{R}$. Then

$$G - \widehat{G} = -\widehat{R}^\dagger \Delta - \Delta^\dagger \widehat{R} - \Delta^\dagger \Delta.$$

Taking operator norms gives Eq. (55). Weyl's eigenvalue inequality gives Eq. (56). In the scalar multiplication case the quadratic form of $R^\dagger R$ on coefficients c is

$$\int_{\mathcal{B}} |r(\mathrm{i}\omega)|^2 \left| \sum_j c_j f_j(\omega) \right|^2 \mathrm{d}\omega,$$

which gives Eq. (57). The operator norm of multiplication by $r - \widehat{r}$ on $L^2(\mathcal{B})$ is its essential supremum, and the finite-grid statement is the scalar sampling theorem applied to the complex error function. □

The data-to-band theorem controls under-sampling of a known complex model; the present test controls whether the model itself is physically compatible with a passive memory. In practice one should report the complex S-parameter fit, its poles, the positivity margin of Σ_r, and the uncertainty of the phase calibration used for the reciprocal read operation.

8 No-go theorem for exact finite passive broadband matching

Finite MR-QM models have rational transfer functions. This is true whether the finite modes are empty resonators, single atoms in resonators, or finite collective atomic spectral bins. The next theorem states a limitation that is often hidden in numerical optimization.

Theorem 10 (No finite exact continuous-band perfect memory)**.** *Let $r(s)$ be the prompt reflection coefficient of a finite, stable, time-independent, passive one-port MR-QM. Suppose that $r(s)$ is analytic in a neighbourhood of the imaginary-axis interval $\mathrm{i}\mathcal{B} = \{\mathrm{i}\omega : \omega \in (\omega_1, \omega_2)\}$ and that $\omega_1 < \omega_2$. If*

$$r(\mathrm{i}\omega) = 0 \quad \textit{for all } \omega \in (\omega_1, \omega_2), \tag{59}$$

then $r(s) \equiv 0$ as a meromorphic function. But any finite resonator realization satisfies $r(s) \to 1$ as $|s| \to \infty$. Hence no such finite passive device can be exactly reflectionless on a nonzero continuous band.

Proof. A finite stable realization has poles only in the open left half-plane, after including positive damping, so r is analytic across the specified imaginary-axis interval. The set of zeros has an accumulation point inside the analytic domain. By the identity theorem, r vanishes identically on the connected analytic domain and therefore as a meromorphic function. On the other hand, Eq. (1) has

$$\lim_{|s|\to\infty} r(s) = 1 \tag{60}$$

because $\Sigma(s) = O(1/s)$ for a finite passive oscillator network. This contradiction proves the result. □

Corollary 2. *Claims of exactly unit memory efficiency over a finite continuous bandwidth in a finite passive time-independent multiresonator system must involve at least one of the following: an approximation, a finite-dimensional signal alphabet, a continuum/infinite spectral measure, active or time-dependent control during absorption, non-Markovian external coupling, or a convention that omits prompt reflection/loss.*

This theorem is not pessimistic. It is the correct starting point for design. It says that finite MR-QM is a broadband matching problem of the Bode–Fano/Darlington type, not an exact algebraic cancellation problem [28, 29]. The figure of merit is the best achievable reflection norm on the target signal set.

9 Bode–Fano area law

The no-go theorem forbids exact zero reflection on a continuous band. A stronger statement is available for passive one-port memories with fixed external coupling: the total logarithmic matching area is finite. This is the memory form of the Bode–Fano limitation [20, 21].

Theorem 11 (Bode–Fano area law for passive MR-QM)**.** *Consider a rational, lossless, passive one-port MR-QM with external coupling κ, reflection coefficient*

$$r(s) = 1 - \frac{\kappa}{s} + O(s^{-2}), \qquad s \to \infty, \tag{61}$$

and no singular inner factor. Boundary zeros on the imaginary axis are allowed only when the logarithmic singularity is integrable, as in the limiting examples used below. Let z_j be the zeros of r in the open right half-plane, counted with multiplicity. Then

$$\int_{-\infty}^{\infty} \log \frac{1}{|r(\mathrm{i}\omega)|}\, \mathrm{d}\omega = \pi \left(\kappa - 2 \sum_j \operatorname{Re} z_j \right) \le \pi\kappa. \tag{62}$$

Consequently, if $|r(\mathrm{i}\omega)| \le \rho$ for all $|\omega| \le B$, then

$$\rho \ge \exp\Big[-\frac{\pi\kappa}{2B}\Big], \qquad \eta_{\mathrm{w}}^{\min} \le 1 - \exp\Big[-\frac{\pi\kappa}{B}\Big]. \tag{63}$$

Proof. The passive one-port reflection coefficient is a rational Schur function in the right half-plane. First assume that it has no boundary zeros; the stated formula with integrable boundary zeros follows by moving the contour a distance $\epsilon > 0$ into the right half-plane and then taking $\epsilon \downarrow 0$. Factor its right-half-plane zeros by the Blaschke product

$$B_r(s) = \prod_j \frac{s - z_j}{s + \bar{z}_j}, \tag{64}$$

which has unit modulus on the imaginary axis. The quotient $g(s) = r(s)/B_r(s)$ is zero-free and Schur in the right half-plane. Applying the Poisson representation to $\log|g|$ at a real point $x > 0$ gives

$$\log|r(x)| - \sum_j \log\left|\frac{x - z_j}{x + \bar{z}_j}\right| = \frac{x}{\pi} \int_{-\infty}^{\infty} \frac{\log|r(\mathrm{i}\omega)|}{x^2 + \omega^2}\, \mathrm{d}\omega. \tag{65}$$

Using $r(x) = 1 - \kappa/x + O(x^{-2})$ and

$$\log\left|\frac{x - z_j}{x + \bar{z}_j}\right| = -\frac{2\operatorname{Re} z_j}{x} + O(x^{-2})$$

and then multiplying by πx and taking $x \to \infty$ yields Eq. (62). Since $|r(\mathrm{i}\omega)| \le 1$ for a lossless passive one-port, the left hand side is nonnegative and bounded above by $\pi\kappa$. If $|r| \le \rho$ on an interval of length $2B$, then

$$2B \log(1/\rho) \le \int_{-\infty}^{\infty} \log|r(\mathrm{i}\omega)|^{-1}\, \mathrm{d}\omega \le \pi\kappa,$$

which gives Eq. (63). □

For the normalized numerical examples below, $\kappa = 2$ and $B = 1$, so Eq. (63) gives $\rho \ge e^{-\pi} = 0.043214$ and $\eta_{\mathrm{w}}^{\min} \le 1 - e^{-2\pi} = 0.998133$. Thus the remaining gap between the finite-mode designs and unity is not merely a numerical imperfection; it is bounded from below by a one-port matching area law unless time-dependence, gain, additional external ports, or a different resource class is introduced.

10 Dynamic bypass of the stationary bound

The Bode–Fano area law applies to linear time-independent passive one-port matching. It does not forbid exact absorption of a known temporal mode when a control waveform changes the coupling in time. This distinction is central for interpreting "universal interface" claims.

Theorem 12 (Gauge-complete exact dynamic capture of one known temporal mode)**.** *Let f be a normalized, piecewise C^1 input envelope on $(-\infty, T)$, and define*

$$E(t) = \int_{-\infty}^{t} |f(s)|^2 \, \mathrm{d}s. \tag{66}$$

On every interval where $E(t) > 0$ and $f(t) \neq 0$, write $f(t) = |f(t)|e^{\mathrm{i}\phi(t)}$. Consider a one-sided memory mode with tunable external coupling and detuning,

$$\dot{a}(t) = -\left[\frac{\kappa(t)}{2} + \mathrm{i}\Delta(t)\right] a(t) - \sqrt{\kappa(t)}\, f_{\mathrm{in}}(t), \tag{67}$$

$$f_{\mathrm{out}}(t) = f_{\mathrm{in}}(t) + \sqrt{\kappa(t)}\, a(t). \tag{68}$$

Choose

$$\kappa(t) = \frac{|f(t)|^2}{E(t)}, \qquad \Delta(t) = -\dot{\phi}(t), \tag{69}$$

with arbitrary bounded interpolation through isolated zeros of f. Then the input $f_{\mathrm{in}} = f$ is captured with $f_{\mathrm{out}}(t) = 0$ for all $t < T$, and

$$a(t) = -\sqrt{E(t)}\, e^{\mathrm{i}\phi(t)}, \qquad |a(t)|^2 = E(t). \tag{70}$$

Thus $\lim_{t\to T} |a(t)|^2 = 1$ if the pulse is fully contained before T. For merely L^2 envelopes the statement holds by approximating f by smooth compactly supported envelopes and taking the L^2-limit of the input–output map.

Proof. The zero-output condition is $\sqrt{\kappa}a = -f$. With Eq. (69) it gives the displayed trajectory and $|a|^2 = E$. Differentiating $a = -\sqrt{E}\, e^{\mathrm{i}\phi}$ gives

$$\dot{a} = \left(\frac{\dot{E}}{2E} + \mathrm{i}\dot{\phi}\right) a = \left(\frac{\kappa}{2} + \mathrm{i}\dot{\phi}\right) a,$$

because $\dot{E} = |f|^2 = \kappa E$. The right hand side of Eq. (67) evaluated on the zero-output trajectory is

$$-\left(\frac{\kappa}{2} + \mathrm{i}\Delta\right) a - \sqrt{\kappa} f = -\left(\frac{\kappa}{2} + \mathrm{i}\Delta\right) a + \kappa a = \left(\frac{\kappa}{2} - \mathrm{i}\Delta\right) a.$$

The choice $\Delta = -\dot{\phi}$ makes the two expressions identical. The energy identity then follows either from the trajectory or from the lossless input–output balance

$$\frac{\mathrm{d}}{\mathrm{d}t}|a(t)|^2 = |f_{\mathrm{in}}(t)|^2 - |f_{\mathrm{out}}(t)|^2.$$

□

Equation (69) is the time-domain counterpart of impedance matching, but the theorem now exposes the full control requirement: the amplitude law fixes the storage probability and the detuning or coupling phase fixes the optical phase. It is exact for a known pulse but depends on the pulse shape, the causal accumulated energy, and the calibrated phase convention. Related dynamic absorption and linewidth-modulation ideas appear in single-photon absorption, short-pulse impedance matching, and recent spin-ensemble absorption–emission optimization [23, 24,

22]. For pulses with an infinite leading tail, $E(t)$ is exponentially small in the far past and the ideal $\kappa(t)$ can become unbounded; practical schedules therefore require either a regularized leading-tail construction or an explicit bounded-control leakage certificate. Thus dynamic matching does not provide a time-independent broadband interface for arbitrary unknown waveforms. It is the first element of the hierarchy: dynamic control gives exact matching on a specified one-dimensional signal space, while the positive-real minimax theory solves the stationary finite-band problem.

Proposition 3 (Capped dynamic-control certificate)**.** *Let f be a normalized input mode and let bounded measurable controls $\kappa_c(t) \geq 0$ and $\Delta_c(t)$ be used in Eq. (67) instead of the ideal controls (69). If the memory mode is initially empty and there is no internal loss, then the actually achieved write efficiency is exactly*

$$\eta_c(T) = |a(T)|^2 = 1 - \int_{-\infty}^{T} |f_{\mathrm{out}}(t)|^2 \,\mathrm{d}t - \int_{T}^{\infty} |f_{\mathrm{in}}(t)|^2 \,\mathrm{d}t. \tag{71}$$

In particular, a hardware-limited capped approximation to the singular ideal law is certified by direct integration of the same input–output equations; it is not certified by the formal ideal waveform alone.

Proof. For Eq. (67) with arbitrary real κ_c, Δ_c,

$$\frac{\mathrm{d}}{\mathrm{d}t}|a(t)|^2 = |f_{\mathrm{in}}(t)|^2 - |f_{\mathrm{out}}(t)|^2.$$

Integrating from the remote past, where $a = 0$, to T gives Eq. (71). The detuning changes phase but not the energy balance. Thus every bounded-control schedule has an experimentally checkable leakage certificate. □

10.1 Exact dynamic capture of a finite temporal alphabet

The one-mode construction has a matrix generalization. It is the constructive counterpart of the rank-capacity theorem.

Theorem 13 (Exact dynamic capture of a finite alphabet)**.** *Let $f_1, \ldots, f_K$ be orthonormal temporal modes and define the column vector*

$$\boldsymbol{f}(t) = (f_1(t), \ldots, f_K(t))^{\mathsf{T}}. \tag{72}$$

Assume that the accumulated Gram matrix

$$S(t) = \int_{-\infty}^{t} \boldsymbol{f}(s)\boldsymbol{f}(s)^{\dagger} \,\mathrm{d}s \tag{73}$$

is nonsingular on the interval of interest; otherwise one uses the regularized seed construction of Appendix D. Consider a passive time-dependent one-input memory with K storage modes,

$$\dot{\boldsymbol{a}}(t) = -\left[\frac{1}{2}\boldsymbol{L}(t)\boldsymbol{L}(t)^{\dagger} + \mathrm{i}H(t)\right]\boldsymbol{a}(t) - \boldsymbol{L}(t)f_{\mathrm{in}}(t), \tag{74}$$

$$f_{\mathrm{out}}(t) = f_{\mathrm{in}}(t) + \boldsymbol{L}(t)^{\dagger}\boldsymbol{a}(t), \tag{75}$$

where $H(t) = H(t)^{\dagger}$ is an optional internal Hamiltonian gauge. There exists a complex coupling waveform $\boldsymbol{L}(t)$ and, if desired, an equivalent real-coupling representation with a Hamiltonian gauge, such that every input

$$f_{\mathrm{in}}(t) = \boldsymbol{f}(t)^{\dagger}\boldsymbol{c}, \qquad \boldsymbol{c} \in \mathbb{C}^K, \tag{76}$$

is captured with $f_{\mathrm{out}}(t) = 0$ and final storage amplitude

$$\boldsymbol{a}(\infty) = U\boldsymbol{c}, \tag{77}$$

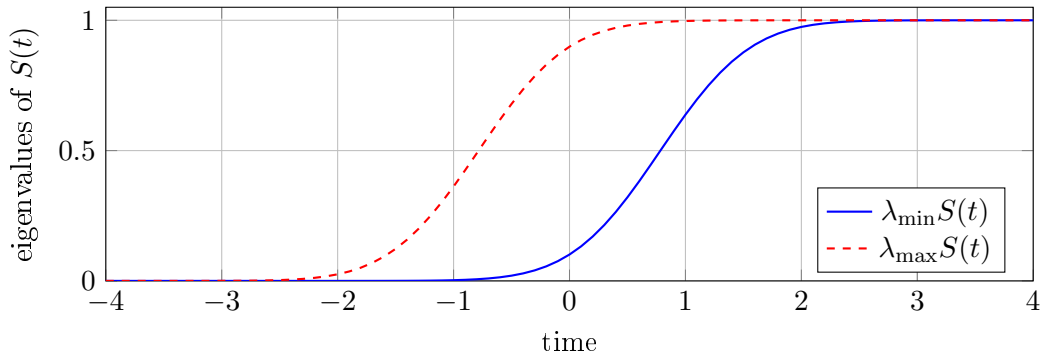

Figure 2: Accumulated Gram eigenvalues for a two-mode Hermite–Gaussian alphabet. Exact dynamic alphabet capture becomes well conditioned only after the accumulated Gram matrix is nonsingular; the regularized seed construction controls the leading singular interval.

where U is a unitary matrix determined by the storage gauge. One explicit zero-output construction is

$$\dot{A}(t) = \frac{1}{2} A(t)^{-\dagger} \boldsymbol{f}(t) \boldsymbol{f}(t)^{\dagger}, \qquad \boldsymbol{L}(t) = -A(t)^{-\dagger} \boldsymbol{f}(t), \qquad H(t) = 0, \tag{78}$$

with $A(t)^{\dagger} A(t) = S(t)$ and $\boldsymbol{a}(t) = A(t)\boldsymbol{c}$. Equivalently, a prescribed differentiable storage-frame rotation $A(t) \mapsto A(t)U(t)$ is implemented by the corresponding Hermitian gauge Hamiltonian.

Proof. For $\boldsymbol{a} = A\boldsymbol{c}$ and $f_{\mathrm{in}} = \boldsymbol{f}^{\dagger}\boldsymbol{c}$, the zero-output condition is

$$\boldsymbol{L}^{\dagger} A = -\boldsymbol{f}^{\dagger}, \tag{79}$$

which is satisfied by $\boldsymbol{L} = -A^{-\dagger}\boldsymbol{f}$. Substitution into Eq. (74) with $H = 0$ gives

$$\dot{A} = -\frac{1}{2}\boldsymbol{L}\boldsymbol{L}^{\dagger} A - \boldsymbol{L}\boldsymbol{f}^{\dagger} = \frac{1}{2} A^{-\dagger} \boldsymbol{f}\boldsymbol{f}^{\dagger},$$

which is Eq. (78). The stored Gram matrix obeys

$$\frac{\mathrm{d}}{\mathrm{d}t}(A^{\dagger}A) = \dot{A}^{\dagger}A + A^{\dagger}\dot{A} = \boldsymbol{f}\boldsymbol{f}^{\dagger}.$$

Thus $A^{\dagger}A = S$ whenever this holds at the initial regularized time. Since the modes are orthonormal, $S(\infty) = I_K$, so $A(\infty)$ is unitary. A time-dependent storage-frame rotation can be implemented after capture or, in an orthonormal register basis, by adding the corresponding Hermitian control Hamiltonian. The zero-output identity and the Gram evolution are unchanged. This shows that phase and basis gauges are physical control requirements, not hidden assumptions. □

The theorem is deliberately resource-explicit. Exact finite-alphabet universality requires a storage dimension at least equal to the alphabet dimension and a calibrated vector coupling waveform. Without those resources, one returns to the stationary positive-real approximation problem and to the Bode–Fano area law.

Corollary 3 (No contradiction with Bode–Fano)**.** *The exact dynamic capture law (69) does not violate Theorem 11, because the system is not time independent and has no stationary reflection coefficient $r(\mathrm{i}\omega)$ to which the Bode–Fano integral applies.*

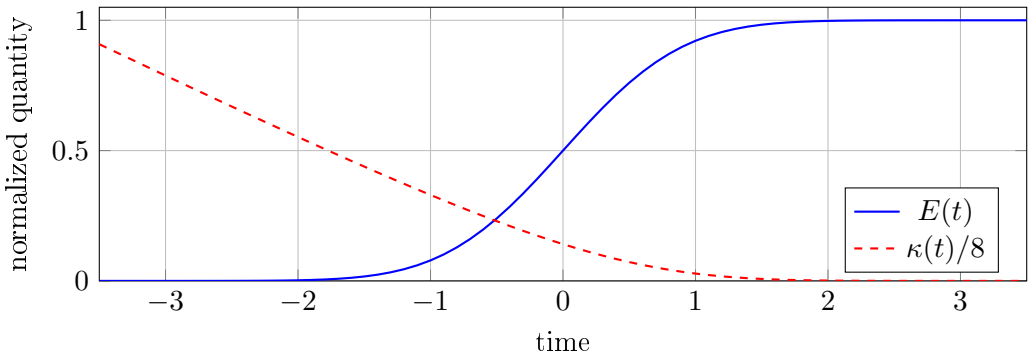

Figure 3: Exact dynamic capture of a chirped Gaussian temporal mode. The accumulated stored energy is $E(t)$ and the impedance-matching law is $\kappa(t) = |f(t)|^2/E(t)$; the plotted coupling is rescaled by a factor eight.

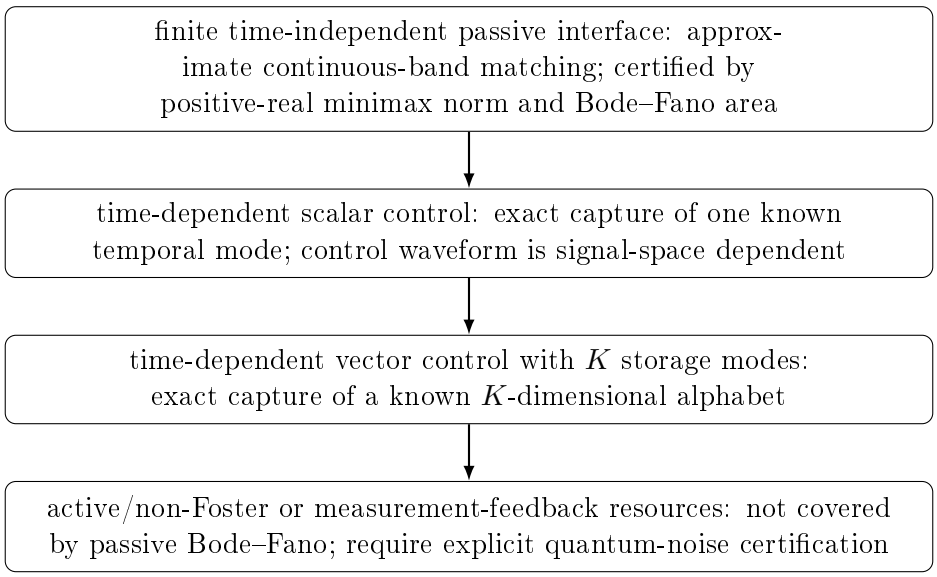

Figure 4: Operational hierarchy. The resources that evade stationary Bode–Fano limitations are precisely the resources that must be reported: time dependence, alphabet dimension, active elements, and added noise.

11 Spectral-admittance synthesis

11.1 Admittance target

Equation (1) can be written as

$$r(s) = \frac{N(s)}{D(s)}, \qquad N(s) = s - \frac{\kappa - \gamma_c}{2} + \Sigma(s), \qquad D(s) = s + \frac{\kappa + \gamma_c}{2} + \Sigma(s). \tag{80}$$

Broadband matching is the problem of making $N(\mathrm{i}\omega)$ small while keeping $D(\mathrm{i}\omega)$ stable and away from zero. The ideal boundary condition is

$$\Sigma(\mathrm{i}\omega + 0) = \frac{\kappa - \gamma_c}{2} - \mathrm{i}\omega, \qquad \omega \in \mathcal{B}. \tag{81}$$

A finite positive-real self-energy cannot satisfy this on a continuous band, but it can approximate it.

Definition 1 (MR-QM spectral synthesis problem). *For a target band $\mathcal{B}$, controlled parasitic loss bound γ_{loss}, and allowed number of auxiliary resonator/matter poles N, find a positive-real*

rational self-energy Σ_N of the form realizable by Eq. (14) that minimizes

$$\epsilon_N(\mathcal{B}) = \operatorname*{ess\,sup}_{\omega\in\mathcal{B}} \left| \frac{\mathrm{i}\omega - \frac{\kappa-\gamma_c}{2} + \Sigma_N(\mathrm{i}\omega)}{\mathrm{i}\omega + \frac{\kappa+\gamma_c}{2} + \Sigma_N(\mathrm{i}\omega)} \right|. \tag{82}$$

The worst-case write efficiency is then $1-\epsilon_N^2$ in the lossless case.

This is the universal finite-device problem. It can be solved by positive-real rational approximation, by a constrained Remez algorithm, by semidefinite KYP constraints, or by direct physical-parameter optimization. The choice of numerical method does not change the physical theory.

11.2 Physical realizability of rational solutions

Theorem 14 (Positive-real synthesis implies physical MR-QM realization)**.** *Let $\Sigma_N(s)$ be a rational positive-real function with real symmetry, poles in the closed left half-plane, and $\Sigma_N(s)\to 0$ as $|s|\to\infty$. Then there exists a passive finite network of harmonic modes coupled to the common resonator whose eliminated self-energy is $\Sigma_N(s)$. If the residues are simple and positive after diagonalization, the realization can be chosen as independent auxiliary resonators; otherwise it is realized as a lossless coupled-resonator network followed by diagonal damping channels. Quantization of this passive network gives a physically realizable linear quantum system with the reflection coefficient (1).*

Proof. Classical Cauer–Foster–Darlington synthesis realizes every rational positive-real driving-point admittance as a passive network of reactive elements and resistive terminations. Replacing each reactive normal mode by a harmonic oscillator and each resistive termination by a Markov input-output channel gives the passive quantum linear realization. Equivalently, the lossless bounded-real transfer function $r(s)$ is the scattering matrix of a passive linear quantum system, and Σ_N is the corresponding Schur complement. The independent-oscillator realization is obtained when the spectral measure of Σ_N is diagonal with positive residues; otherwise a unitary transformation gives coupled resonators with the same admittance. □

This theorem is the mathematical content behind the statement that MR-QM is a universal interface. The universality is spectral: once a positive-real admittance is specified, the same memory response can be implemented with microwave CPW resonators, optical microrings, photonic molecules, rare-earth ensembles, spin ensembles, or hybrid systems, limited only by fabrication losses and controllability.

11.3 Continuum ideal and finite approximation

In the continuum limit the finite sum in Eq. (14) is replaced by a positive spectral measure μ:

$$\Sigma_\mu(s) = \int_{\mathbb{R}} \frac{\mathrm{d}\mu(\nu)}{s+\Gamma(\nu)+\mathrm{i}\nu}, \qquad \mathrm{d}\mu(\nu)\ge 0, \quad \Gamma(\nu)\ge 0. \tag{83}$$

The boundary matching equation is the singular integral system

$$\int \frac{\Gamma(\nu)\,\mathrm{d}\mu(\nu)}{\Gamma(\nu)^2+(\omega+\nu)^2} = \frac{\kappa-\gamma_c}{2}, \tag{84}$$

$$\omega - \int \frac{(\omega+\nu)\,\mathrm{d}\mu(\nu)}{\Gamma(\nu)^2+(\omega+\nu)^2} = 0, \qquad \omega\in\mathcal{B}. \tag{85}$$

Equations (84)–(85) are the exact continuum spectral-admittance conditions. They are the analogue of designing an exactly matched continuous transmission-line load. A finite MR-QM is a quadrature approximation of μ plus a finite positive-real correction.

11.4 Existence and density of resource-constrained synthesis

The continuum equations are useful only if the corresponding optimization problem is mathematically closed. The physically correct closure is not an unconstrained measure on the whole plane, but a fabrication box and an oscillator-strength budget. Let

$$\mathfrak{K} = [\Gamma_{\min}, \Gamma_{\max}] \times [-\Delta_{\max}, \Delta_{\max}], \qquad 0 < \Gamma_{\min} < \Gamma_{\max} < \infty, \tag{86}$$

and let $\mathcal{M}_+(\mathfrak{K}; M)$ be the positive Borel measures on $\mathfrak{K}$ with total mass at most M. For $\mu \in \mathcal{M}_+(\mathfrak{K}; M)$ set

$$\Sigma_\mu(s) = \int_{\mathfrak{K}} \frac{\mathrm{d}\mu(\Gamma, \nu)}{s + \Gamma + \mathrm{i}\nu}. \tag{87}$$

The resource-constrained design problem is

$$\rho_\star = \inf_{\mu \in \mathcal{M}_+(\mathfrak{K}; M)} \sup_{\omega \in \mathcal{B}} \left| \frac{\mathrm{i}\omega - \kappa/2 + \gamma_c/2 + \Sigma_\mu(\mathrm{i}\omega)}{\mathrm{i}\omega + \kappa/2 + \gamma_c/2 + \Sigma_\mu(\mathrm{i}\omega)} \right|. \tag{88}$$

Theorem 15 (Existence and finite-mode density)**.** *For every compact signal band $\mathcal{B}$ and every finite resource box $\mathfrak{K}, M$, the minimization problem (88) has a minimizer. Moreover, for every admissible continuum measure μ and every $\epsilon > 0$ there is a finite atomic measure*

$$\mu_N = \sum_{n=1}^{N} w_n \delta_{(\Gamma_n, \nu_n)}, \qquad w_n > 0, \tag{89}$$

such that the associated finite MR-QM satisfies

$$\sup_{\omega \in \mathcal{B}} |r_{\mu_N}(\mathrm{i}\omega) - r_\mu(\mathrm{i}\omega)| < \epsilon. \tag{90}$$

Proof. The set $\mathcal{M}_+(\mathfrak{K}; M)$ is weak-star compact because $\mathfrak{K}$ is compact and the masses are uniformly bounded. For each $\omega \in \mathcal{B}$ the kernel $(\Gamma, \nu) \mapsto (\mathrm{i}\omega + \Gamma + \mathrm{i}\nu)^{-1}$ is continuous and uniformly bounded by $\Gamma_{\min}^{-1}$, hence $\Sigma_{\mu_n}(\mathrm{i}\omega) \to \Sigma_\mu(\mathrm{i}\omega)$ uniformly on $\mathcal{B}$ whenever $\mu_n \to \mu$ weak-star. The denominator of the Cayley transform is uniformly separated from zero since

$$\mathrm{Re}\left[\frac{\kappa + \gamma_c}{2} + \Sigma_\mu(\mathrm{i}\omega)\right] \geq \frac{\kappa + \gamma_c}{2} > 0. \tag{91}$$

Therefore $\mu \mapsto \sup_{\omega \in \mathcal{B}} |r_\mu(\mathrm{i}\omega)|$ is continuous on the compact admissible set, so a minimizer exists. Finally, finite positive atomic measures are weak-star dense in positive measures on a compact metric space; applying the same uniform-continuity argument to the Cayley transform gives (90). □

This theorem is the formal reason why finite multiresonator synthesis is a controlled approximation rather than a heuristic. Increasing the number of resonators is a quadrature refinement of a positive-real continuum optimum, while the no-go theorem states that the limiting optimum cannot be made exactly zero on a continuous band unless an infinite or time-dependent resource is admitted.

11.5 Finite-grid Carathéodory certificate

The continuum minimizer in Eq. (88) is conceptually useful, but every experiment and numerical certificate uses finitely many frequency samples. On a finite grid, no continuum of atoms is required.

Theorem 16 (Sparse atomic certificate on a frequency grid). *Let $\Omega_L = \{\omega_1, \dots, \omega_L\}$ be a finite frequency grid, and let $\mu \in \mathcal{M}_+(\mathfrak{K}; M)$ be any admissible positive measure. There exists an atomic measure*

$$\mu_{\mathrm{sp}} = \sum_{n=1}^{N_{\mathrm{sp}}} w_n \delta_{(\Gamma_n, \nu_n)}, \qquad N_{\mathrm{sp}} \le 2L + 1, \tag{92}$$

such that

$$\Sigma_{\mu_{\mathrm{sp}}}(\mathrm{i}\omega_\ell) = \Sigma_\mu(\mathrm{i}\omega_\ell), \qquad \ell = 1, \dots, L, \tag{93}$$

and $\mu_{\mathrm{sp}}(\mathfrak{K}) = \mu(\mathfrak{K}) \le M$. Therefore the reflection coefficient, the grid epigraph constraints, and every grid-certified write efficiency are identical for μ and μ_{sp} on Ω_L.

Proof. Define the continuous feature map

$$\Phi(\Gamma, \nu) = \left(\mathrm{Re}\, \frac{1}{\mathrm{i}\omega_1 + \Gamma + \mathrm{i}\nu}, \mathrm{Im}\, \frac{1}{\mathrm{i}\omega_1 + \Gamma + \mathrm{i}\nu}, \dots, \mathrm{Re}\, \frac{1}{\mathrm{i}\omega_L + \Gamma + \mathrm{i}\nu}, \mathrm{Im}\, \frac{1}{\mathrm{i}\omega_L + \Gamma + \mathrm{i}\nu}, 1 \right) \in \mathbb{R}^{2L+1}. \tag{94}$$

The vector

$$y = \int_{\mathfrak{K}} \Phi(\Gamma, \nu)\, \mathrm{d}\mu(\Gamma, \nu)$$

belongs to the conic hull of $\Phi(\mathfrak{K}) \subset \mathbb{R}^{2L+1}$. By the conic Carathéodory theorem, y is a nonnegative linear combination of at most $2L+1$ points of $\Phi(\mathfrak{K})$. The corresponding coefficients and support points define μ_{sp}. Equality of the first $2L$ coordinates gives equality of the real and imaginary parts of Σ on the grid, and equality of the last coordinate preserves the mass budget. □

This is a useful certification theorem rather than an efficient design algorithm. It says that a grid-certified continuum optimum always has a finite sparse witness. The remaining task is to find a good witness with a stable and experimentally realistic pole geometry.

11.6 Finite positive-real Remez synthesis

For a fixed finite pole class Eq. (148), the practical problem is the epigraph program

$$\begin{aligned} \text{minimize} \quad & \rho, && (95)\\ \text{subject to} \quad & |r(\mathrm{i}\omega_\ell; \boldsymbol{p})| \le \rho, \qquad \ell = 1, \dots, L, && (96)\\ & \Gamma_j > 0, \quad w_j > 0, \quad \Delta_j > 0. && (97) \end{aligned}$$

The grid constraints are nonlinear but low dimensional, and positivity is enforced by logarithmic variables. After optimization on a grid, the result must be certified on an independent dense grid and by direct integration of the passive dilation. The near-equiripple envelope of the certified solutions below is the positive-real analogue of classical Chebyshev/Remez filter synthesis.

12 Local flat matching and relation to known MR-QM conditions

12.1 Derivative hierarchy

Let $s_0 = \mathrm{i}\omega_0$ be the centre of the signal band. If $D(s_0) \neq 0$, then a zero of $r(s)$ of order $p+1$ at s_0 is equivalent to

$$N^{(q)}(s_0) = 0, \qquad q = 0, 1, \dots, p. \tag{98}$$

Using Eq. (80) gives the hierarchy

$$\begin{aligned} \Sigma(s_0) &= \frac{\kappa - \gamma_c}{2} - s_0, && (99)\\ \Sigma'(s_0) &= -1, && (100)\\ \Sigma^{(q)}(s_0) &= 0, \qquad q = 2, \dots, p. && (101) \end{aligned}$$

Equation (99) is the ordinary impedance matching condition. Equation (100) cancels the first-order spectral phase dispersion of the common resonator; it is the local form of white-cavity or spectral matching. Higher equations impose progressively flatter reflection.

For a symmetric diagonal resonator spectrum

$$\Sigma(s) = \frac{w_0}{s+\Gamma_0} + \sum_{j=1}^{J} w_j \left[\frac{1}{s+\Gamma_j + \mathrm{i}\Delta_j} + \frac{1}{s+\Gamma_j - \mathrm{i}\Delta_j} \right], \qquad w_j > 0, \tag{102}$$

the derivatives are explicit:

$$\Sigma^{(q)}(0) = (-1)^q q! \left[\frac{w_0}{\Gamma_0^{q+1}} + \sum_{j=1}^{J} w_j \left(\frac{1}{(\Gamma_j + \mathrm{i}\Delta_j)^{q+1}} + \frac{1}{(\Gamma_j - \mathrm{i}\Delta_j)^{q+1}} \right) \right]. \tag{103}$$

Thus flat matching is a finite system of real algebraic equations in positive linewidths, detunings and oscillator strengths.

12.2 Recovery of standard impedance conditions

If all auxiliary resonators are empty and form a spatial-frequency comb directly coupled to the waveguide, the self-energy becomes the comb Green function. For a periodic array the rephasing time is $T = 2\pi/\Delta$, and the waveguide coupling linewidth is $\Gamma = 2\pi g^2/c$. Moiseev's Bragg condition

$$\Delta = \frac{\pi}{2}\Gamma \tag{104}$$

is precisely the condition that the prompt reflection defect vanish at the comb centre while the resonator phases rephase at the echo time [7]. In the common-resonator formulation the same physics appears as Eq. (99) for the common mode and, when broadband flatness is required, Eq. (100).

For a rectangular distribution of auxiliary resonator frequencies loaded by Lorentzian-broadened atomic ensembles, the recent ensemble theory gives a common-resonator matching condition of the form

$$\kappa = \gamma_c + \frac{2Mg^2}{\delta_{\mathrm{in}} F(\chi\delta_{\mathrm{in}}, \chi\Gamma_\Sigma, 0)}, \tag{105}$$

with a spectral-broadening function $F > 1$ determined by the atomic loading [16]. In the notation of this paper this is simply

$$\kappa = \gamma_c + 2\Sigma(0), \tag{106}$$

while the additional spectral condition derived there is the special rectangular-continuum evaluation of

$$\Sigma'(0) = -1. \tag{107}$$

The spectral-topological conditions of small cascade memories are finite-dimensional versions of the same hierarchy: several tunable poles are moved until the numerator $N(s)$ has a high-order zero or an equal-ripple small norm on the chosen band [11, 10].

13 Retrieval and full memory channel

Write matching is not sufficient for a quantum memory; the absorbed excitation must be emitted on demand with controlled temporal mode, phase and noise. The spectral-admittance theory separates write and read cleanly.

Let $W : \mathcal{H}_{\mathcal{B}} \to \mathcal{H}_{\mathrm{int}}$ be the write map into controlled internal modes. In the lossless case,

$$W^\dagger W = I - R^\dagger R, \tag{108}$$

where R is multiplication by $r(\omega)$ on the input band. Let $U_{\mathrm{s}}(T)$ be the controlled storage evolution, including detuning reversal, spin-wave transfer, AFC rephasing, switch-off of the common resonator, or dynamical decoupling. Let W_{r} be the read map from internal modes to the output channel.

Theorem 17 (Time-reversal retrieval)**.** *Suppose the read Hamiltonian is the antiunitary time reverse of the write Hamiltonian on the controlled internal subspace, and suppose storage control satisfies*

$$U_{\mathrm{s}}(T)Wf = e^{\mathrm{i}\phi}Wf \quad \text{for every } f \in \mathcal{S} \tag{109}$$

on a signal subspace $\mathcal{S}$. Then the full memory channel on $\mathcal{S}$ is

$$f(t) \longmapsto e^{\mathrm{i}\phi} f^*(T_{\mathrm{e}} - t) \tag{110}$$

up to the write/read reflection defects and intrinsic decoherence. In particular, for a lossless perfectly written finite-dimensional subspace the retrieval fidelity is unity, and the total efficiency is the product of write, storage and read efficiencies.

Proof. The passive write dynamics defines a unitary map between input temporal modes and internal normal modes plus prompt output modes. Reversing the detunings and coupling phases implements the inverse unitary on the controlled sector. If $U_{\mathrm{s}}(T)$ rephases the written subspace to a common phase, the read operation is $W^\dagger$ followed by time reversal of the envelope. Orthogonality and phase preservation follow from unitarity. Decoherence multiplies the controlled internal norm by the corresponding survival factor. □

This theorem includes AFC echo retrieval at $T = 2\pi/\Delta$, CRIB/GEM detuning reversal, and switchable-coupler multiresonator protocols as different ways of realizing the same inverse map [4, 5, 6, 12, 13].

13.1 Finite-alphabet Gram certificate

For experiments and network protocols the relevant signal space is often not the full continuous band but a finite alphabet of temporal modes. The spectral theory reduces this problem to a finite matrix.

Theorem 18 (Exact finite-alphabet write certificate)**.** *Let $\mathcal{S} = \mathrm{span}\{f_1, \dots, f_K\} \subset \mathcal{H}_{\mathcal{B}}$, where the f_j are orthonormal spectra. In a lossless controlled-dilation MR-QM the write Gram matrix on $\mathcal{S}$ is*

$$G_{ij} = \langle f_i, W^\dagger W f_j \rangle = \delta_{ij} - \int_{\mathcal{B}} |r(\mathrm{i}\omega)|^2 f_i^*(\omega) f_j(\omega)\, \mathrm{d}\omega. \tag{111}$$

The guaranteed write efficiency on the whole alphabet is

$$\eta_{\min}(\mathcal{S}) = \lambda_{\min}(G), \tag{112}$$

and the Haar-average write efficiency over normalized states in $\mathcal{S}$ is

$$\overline{\eta}(\mathcal{S}) = \frac{1}{K} \operatorname{Tr} G. \tag{113}$$

Perfect write on $\mathcal{S}$ is equivalent to $G = I_K$.

Proof. Theorem 5 gives $W^\dagger W = I - R^\dagger R$, where R is multiplication by r on the signal band. Restriction to the basis f_j gives Eq. (111). For a normalized vector $c \in \mathbb{C}^K$, the stored probability of $f = \sum_j c_j f_j$ is $c^\dagger G c$; minimizing over $\|c\| = 1$ gives the smallest eigenvalue. Averaging $c^\dagger G c$ over the unit sphere gives $\operatorname{Tr} G/K$. Finally, $G = I_K$ is equivalent to $Rf = 0$ for every $f \in \mathcal{S}$. □

This theorem is the finite-dimensional object that should accompany experimental claims of multimode operation. It is stronger than quoting the efficiency of one pulse shape, and it is more realistic than demanding perfect performance on an entire continuum.

13.2 Reciprocal readout and the full memory channel

The write certificate also determines the ideal readout when the storage dilation can be time reversed.

Theorem 19 (Reciprocal readout theorem). *Let $W : \mathcal{S} \to \mathcal{K}$ be the write map from a finite signal alphabet $\mathcal{S}$ into the controlled storage space $\mathcal{K}$, and assume that the read stage is the exact reciprocal time reversal on the range of W. Then the write–read amplitude operator on $\mathcal{S}$ is*

$$M_{\mathrm{rt}} = W^\dagger W = G, \tag{114}$$

where G is the Gram matrix in Theorem 18. Consequently,

$$\eta_{\mathrm{rt}}^{\min}(\mathcal{S}) = \lambda_{\min}(G)^2, \qquad \eta_{\mathrm{rt}}^{\mathrm{avg}}(\mathcal{S}) = \frac{1}{K}\operatorname{Tr} G^2, \tag{115}$$

for the worst-case and Haar-average unconditional round-trip efficiencies on $\mathcal{S}$. If $G = I_K$, the full memory channel is the identity on the alphabet up to a programmable unitary phase convention.

Proof. The controlled dilation is unitary on the direct sum of the signal and storage ports. The reciprocal read operation is obtained by reversing the write Hamiltonian phases and interchanging input and output temporal boundary conditions; on the stored subspace this is the adjoint map $W^\dagger$. Hence the round-trip amplitude is $W^\dagger W$. In the alphabet basis this is exactly the Gram matrix computed in Eq. (111). The singular values of the positive matrix G are its eigenvalues. Therefore the worst-case output probability is $\min_{\|c\|=1} \|Gc\|^2 = \lambda_{\min}(G)^2$, and Haar averaging gives $\operatorname{Tr} G^2/K$. □

This result separates two efficiencies that are often conflated. The write efficiency is governed by G, whereas the unconditional write–read efficiency is governed by G^2 for reciprocal retrieval. Conditional state fidelity after a successful retrieval may be high even when the unconditional probability is reduced; the Gram certificate reports the probability loss without hiding it in postselection.

13.3 Noise-channel certificate

A quantum memory certificate is incomplete unless it specifies noise. In the linear weak-excitation regime the same controlled dilation fixes the noise channel.

Theorem 20 (Noise form of reciprocal MR-QM). *Let the hypotheses of Theorem 19 hold and let G be the finite-alphabet write Gram matrix. In the Heisenberg picture the ideal reciprocal readout channel on the alphabet annihilation vector $\hat{\boldsymbol{a}}$ has the form*

$$\hat{\boldsymbol{a}}_{\mathrm{out}} = G\hat{\boldsymbol{a}}_{\mathrm{in}} + E\hat{\boldsymbol{v}}, \tag{116}$$

where $\hat{\boldsymbol{v}}$ is an environmental bosonic vector and

$$EE^\dagger = I - G^2. \tag{117}$$

Consequently, in the eigenbasis of G the channel is a product of pure-loss channels with transmissivities

$$\tau_\alpha = g_\alpha^2, \qquad 0 \le g_\alpha \le 1, \tag{118}$$

where g_α are the eigenvalues of G. If the environmental modes have normally ordered covariance $\bar{N}_E = \langle \hat{\boldsymbol{v}}^\dagger \hat{\boldsymbol{v}} \rangle$, the added output photon-noise matrix is

$$N_{\mathrm{add}} = E\bar{N}_E E^\dagger. \tag{119}$$

For a K-mode single-photon qudit encoded in $\mathcal{S}$, the unconditional success probability is at least $\lambda_{\min}(G)^2$. The conditional overlap with the intended qudit after a successful readout obeys

$$F_{\mathrm{cond}} \geq \left(\frac{\lambda_{\min}(G)}{\lambda_{\max}(G)}\right)^2. \tag{120}$$

In particular, if the only imperfection is the prompt reflection bound $G \geq \eta_{\min} I$ and $\lambda_{\max}(G) \leq 1$, then $F_{\mathrm{cond}} \geq \eta_{\min}^2$.

Proof. The full signal–storage–environment evolution is unitary, so the output annihilation operators must preserve canonical commutators. The reciprocal amplitude on the alphabet is G by Theorem 19; therefore the remaining environmental term must satisfy Eq. (117). Diagonalizing the positive contraction $G = U\,\mathrm{diag}(g_\alpha)U^\dagger$ reduces Eq. (116) to independent beamsplitter channels with transmissivities g_α^2. Equation (119) is the normally ordered covariance of the environmental contribution. For an input qudit $|\psi\rangle = \sum_\alpha c_\alpha |\alpha\rangle$, the unnormalized retrieved single-photon component is $G|\psi\rangle$. Its probability is $\langle\psi|G^2|\psi\rangle \geq \lambda_{\min}(G)^2$. The conditional overlap with the intended qudit is

$$\frac{|\langle\psi|G|\psi\rangle|^2}{\langle\psi|G^2|\psi\rangle} \geq \frac{\lambda_{\min}(G)^2}{\lambda_{\max}(G)^2},$$

which gives Eq. (120). □

This theorem turns the usual efficiency statement into a quantum-channel statement. Vacuum uncontrolled ports give quantum-limited loss. Thermally occupied microwave or mechanical ports add the normally ordered noise in Eq. (119), which must be reported separately from coherent efficiency.

Theorem 21 (Operational distance to an ideal finite-alphabet memory)**.** *Consider the vacuum-noise reciprocal channel of Theorem 20 on a K-dimensional single-photon alphabet, and let the positive round-trip amplitude be G with eigenvalues $0 \leq g_\alpha \leq 1$. Let $\mathcal{I}$ be the ideal memory channel on the same alphabet, with the loss output treated as an orthogonal erasure flag. Then*

$$P_{\mathrm{succ}}^{\mathrm{wc}} \geq g_{\min}^2, \tag{121}$$

$$F_{\mathrm{e}} = \frac{|\operatorname{Tr} G|^2}{K^2}, \tag{122}$$

$$\overline{F} = \frac{\operatorname{Tr}(G^2) + |\operatorname{Tr} G|^2}{K(K+1)}, \tag{123}$$

$$\|\mathcal{E}_G - \mathcal{I}\|_\diamond \leq 2\sqrt{2(1-g_{\min})}, \tag{124}$$

where $g_{\min} = \lambda_{\min}(G)$. If storage decoherence or readout imbalance is represented by a known contraction D on the stored alphabet, the same formulas hold with G replaced by the singular-value contraction $A = D^{1/2}G$, except that F_{e} and $\overline{F}$ use A and Eq. (124) uses $s_{\min}(A)$.

Proof. A Stinespring isometry for the vacuum pure-loss alphabet channel is

$$V|\psi\rangle = G|\psi\rangle_{\mathrm{out}}|0\rangle_{\mathrm{e}} + (I - G^2)^{1/2}|\psi\rangle_{\mathrm{e}}|\mathrm{er}\rangle_{\mathrm{out}}.$$

The worst-case success probability is $\|G|\psi\rangle\|^2 \geq g_{\min}^2$. The entanglement fidelity follows from the standard Kraus formula; only the no-erasure Kraus operator G overlaps the ideal output, giving Eq. (122). Haar averaging $\int |\langle\psi|G|\psi\rangle|^2 \mathrm{d}\psi$ gives Eq. (123). For every normalized $|\psi\rangle$,

$$\|(V - V_0)|\psi\rangle\|^2 = \|(G - I)|\psi\rangle\|^2 + \|(I - G^2)^{1/2}|\psi\rangle\|^2 \leq (1 - g_{\min})^2 + 1 - g_{\min}^2 = 2(1 - g_{\min}),$$

where $V_0|\psi\rangle = |\psi\rangle_{\mathrm{out}}|0\rangle_{\mathrm{e}}$. The diamond distance between channels is at most twice the operator-norm distance between these Stinespring isometries, which proves Eq. (124). A known storage contraction is absorbed into the no-erasure amplitude A, followed by the same singular-value argument. □

This theorem gives an operational end point for the certificate: the same Gram matrix that reports write and round-trip probabilities also gives entanglement fidelity, average unconditional qudit fidelity and a worst-case channel-norm distance to an ideal memory. It is intentionally conservative, but it is independent of a particular quantum-network protocol.

13.4 Finite-mode capacity of the write map

The same operator formulation gives a sharp finite-dimensional obstruction that is independent of the details of the resonator topology.

Theorem 22 (Rank capacity bound)**.** *Assume that after the write stage the controllable long-lived memory sector is an M-dimensional Hilbert space and that the write operation is passive and lossless except for the prompt output channel. Let $W : \mathcal{H}_{\mathcal{B}} \to \mathbb{C}^M$ be the write map. If K orthonormal input modes $f_1, \dots, f_K$ are written with efficiencies $\eta_j = \|W f_j\|^2$, then*

$$\sum_{j=1}^{K} \eta_j \le M. \tag{125}$$

Consequently, exact unit-efficiency storage of a K-dimensional temporal alphabet requires $K \le M$, and storage with average efficiency at least $1-\epsilon$ requires

$$K(1-\epsilon) \le M. \tag{126}$$

Proof. Passivity gives $0 \le W^\dagger W \le I$ and $\operatorname{rank}(W^\dagger W) \le M$. Therefore $W^\dagger W$ has at most M nonzero eigenvalues, each no larger than one. For $P_K = \sum_{j=1}^{K} |f_j\rangle\langle f_j|$,

$$\sum_{j=1}^{K} \eta_j = \operatorname{Tr}(P_K W^\dagger W P_K) \le \operatorname{Tr}(W^\dagger W) \le M. \tag{127}$$

The two corollaries follow immediately. □

This bound is the finite-mode form of the time-bandwidth limitation. It does not forbid high efficiency on a prescribed finite alphabet, but it forbids interpreting a finite passive memory as an exact isometry on an unlimited continuum of orthogonal temporal modes.

Together with Theorem 12, the rank bound gives the operational universality hierarchy. A known single mode can be captured exactly by scalar time-dependent matching. A K-dimensional known alphabet can be exactly stored by the matrix dynamic construction of Theorem 13 only when the controlled storage dimension is at least K. A continuous band contains infinitely many orthogonal modes and therefore cannot be exactly represented by a finite passive memory; it can only be approximated, with the stationary approximation quality governed by the positive-real minimax and Bode–Fano certificates.

14 Fixed-pole convex synthesis and lower certificates

The nonconvex part of finite positive-real synthesis is the placement of passive poles. Once a pole support is fixed, however, the oscillator-strength subproblem has a convex structure. This observation turns a proposed fixed architecture into a globally checkable certificate rather than a heuristic fit.

Let

$$h_n(\omega) = \frac{1}{\mathrm{i}\omega + \Gamma_n + \mathrm{i}\nu_n}, \qquad \Gamma_n > 0, \tag{128}$$

or a symmetry-constrained real combination such as

$$h_n(\omega) = \frac{1}{\mathrm{i}\omega + \Gamma_n + \mathrm{i}\Delta_n} + \frac{1}{\mathrm{i}\omega + \Gamma_n - \mathrm{i}\Delta_n}. \tag{129}$$

For nonnegative weights $w_n \geq 0$, define

$$\Sigma_w(\mathrm{i}\omega) = \sum_{n=1}^{N} w_n h_n(\omega). \tag{130}$$

Theorem 23 (Fixed-pole convexity). *Fix $0 \leq \rho < 1$ and a finite grid $\Omega_L = \{\omega_\ell\}_{\ell=1}^{L}$. The set of nonnegative oscillator-strength vectors $w \in \mathbb{R}_+^N$ satisfying*

$$|r_w(\mathrm{i}\omega_\ell)| \leq \rho, \qquad \ell = 1, \ldots, L, \tag{131}$$

is convex. More explicitly, Eq. (131) is equivalent to

$$q_\ell(w;\rho) \leq 0, \qquad \ell = 1, \ldots, L, \tag{132}$$

where

$$q_\ell(w;\rho) = |A_\ell + h_\ell^{\mathsf{T}} w|^2 - \rho^2 |B_\ell + h_\ell^{\mathsf{T}} w|^2, \tag{133}$$

$$A_\ell = \mathrm{i}\omega_\ell - \frac{\kappa}{2} + \frac{\gamma_c}{2}, \qquad B_\ell = \mathrm{i}\omega_\ell + \frac{\kappa}{2} + \frac{\gamma_c}{2}, \tag{134}$$

and $h_\ell = (h_1(\omega_\ell), \ldots, h_N(\omega_\ell))^{\mathsf{T}}$. Each q_ℓ has Hessian

$$\nabla^2 q_\ell = 2(1-\rho^2)\,\mathrm{Re}(h_\ell h_\ell^\dagger) \succeq 0. \tag{135}$$

Consequently, for fixed poles the minimum attainable grid reflection norm can be found by bisection in ρ with convex feasibility tests, and any infeasibility dual certificate is a rigorous lower bound for that pole support.

Proof. The denominator of the passive Cayley transform has positive real part on the imaginary axis because $\mathrm{Re}[\kappa/2 + \gamma_c/2 + \Sigma_w(\mathrm{i}\omega)] > 0$, so multiplying $|r_w| \leq \rho$ by the denominator is nonsingular and gives

$$|A_\ell + h_\ell^{\mathsf{T}} w|^2 \leq \rho^2 |B_\ell + h_\ell^{\mathsf{T}} w|^2. \tag{136}$$

Expanding the two squared moduli in the real variables w_n yields q_ℓ. The quadratic part is

$$(1-\rho^2)|h_\ell^{\mathsf{T}} w|^2 = w^{\mathsf{T}} (1-\rho^2)\,\mathrm{Re}(h_\ell h_\ell^\dagger) w, \tag{137}$$

which is positive semidefinite for $\rho < 1$. Hence each sublevel set $q_\ell(w;\rho) \leq 0$ is convex, and the intersection with the positive orthant is convex. Feasibility is monotone in ρ, giving the bisection statement. □

This theorem separates discovery from certification. Nonlinear search may be used to find useful pole locations, but once a fixed support is proposed, the best nonnegative weights and the lower bound for that support are globally certifiable.

For implementation, write

$$Q_\ell = (1-\rho^2)\,\mathrm{Re}(h_\ell h_\ell^\dagger), \tag{138}$$

$$b_\ell = \mathrm{Re}\{(A_\ell - \rho^2 B_\ell)^* h_\ell\}, \tag{139}$$

$$c_\ell = |A_\ell|^2 - \rho^2 |B_\ell|^2, \tag{140}$$

so that

$$q_\ell(w;\rho) = w^{\mathsf{T}} Q_\ell w + 2 b_\ell^{\mathsf{T}} w + c_\ell. \tag{141}$$

A large grid can be handled by cutting planes: solve on a coarse grid, add the dense-grid frequency with largest violation, and iterate until the independent dense-grid violation is below tolerance.

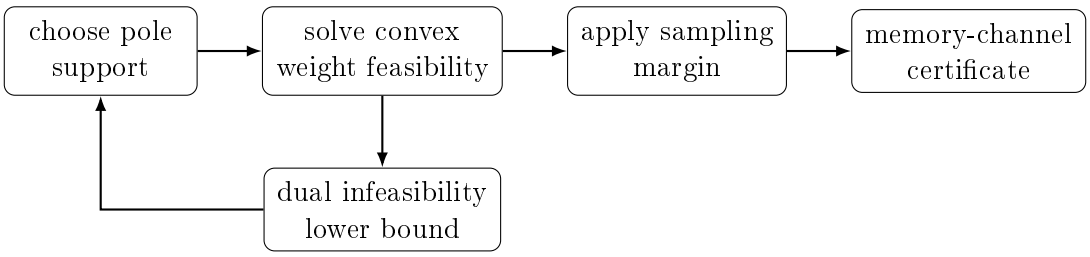

Figure 5: Fixed-support certification workflow. Pole discovery is geometric and may be nonconvex, but the oscillator-strength certificate for a proposed support is a convex feasibility problem with checkable lower bounds.

15 Deterministic robustness certificate

Monte-Carlo fabrication studies are useful but not sufficient for certification. The spectral-admittance form gives a deterministic perturbation bound.

Theorem 24 (Self-energy perturbation bound)**.** *On a compact band $\mathcal{B}$, define*

$$D(\omega) = \mathrm{i}\omega + \frac{\kappa + \gamma_c}{2} + \Sigma(\mathrm{i}\omega), \qquad d = \inf_{\omega\in\mathcal{B}} |D(\omega)|. \tag{142}$$

Let a perturbed device have self-energy $\Sigma + \delta\Sigma$ with

$$\epsilon = \sup_{\omega\in\mathcal{B}} |\delta\Sigma(\mathrm{i}\omega)| < d. \tag{143}$$

Then

$$\sup_{\omega\in\mathcal{B}} |r_{\Sigma+\delta\Sigma}(\mathrm{i}\omega) - r_\Sigma(\mathrm{i}\omega)| \le \frac{\kappa\epsilon}{d(d-\epsilon)}. \tag{144}$$

If $\rho = \sup_{\omega\in\mathcal{B}} |r_\Sigma(\mathrm{i}\omega)|$, the perturbed worst-case write efficiency satisfies

$$\eta_{\mathrm{w}}^{\min}(\Sigma + \delta\Sigma) \ge 1 - \left(\rho + \frac{\kappa\epsilon}{d(d-\epsilon)}\right)^2. \tag{145}$$

Proof. For fixed ω write

$$r_\Sigma = \frac{N + \Sigma}{D}, \qquad r_{\Sigma+\delta\Sigma} = \frac{N + \Sigma + \delta\Sigma}{D + \delta\Sigma},$$

where $N = \mathrm{i}\omega - \kappa/2 + \gamma_c/2$ and $D = \mathrm{i}\omega + \kappa/2 + \gamma_c/2 + \Sigma$. A direct subtraction gives

$$r_{\Sigma+\delta\Sigma} - r_\Sigma = \frac{\kappa\,\delta\Sigma}{D(D + \delta\Sigma)}. \tag{146}$$

Since $|D| \ge d$ and $|D + \delta\Sigma| \ge d - \epsilon$, Eq. (144) follows. The efficiency bound is the triangle inequality applied to $\sup |r|$. □

The bound is conservative but deterministic. It converts a calibrated admissible self-energy error into a guaranteed lower efficiency without assuming a probability distribution over fabrication errors.

16 Numerical certification of the finite-mode synthesis

This section gives a reproducible numerical check of the preceding theory. The purpose is not to claim a globally optimal experimental design, but to verify the certification chain: positive-real passivity on the boundary and in the open right half-plane, Schur contractivity, causal Schur-to-admittance inversion, minimum-phase/all-pass ambiguity, complex-response uncertainty propagation with full out-of-alphabet prompt leakage, operational finite-alphabet channel distance, the exact spectral energy identity, the Bode–Fano area constraint, the superiority of finite-band minimax matching over local Taylor cancellation, controlled-dilation consistency, deterministic self-energy robustness, Monte-Carlo robustness under fabrication errors, data-to-band measurement margins, capped dynamic-control leakage, and thermal-noise conversion into added output photons.

We work in normalized units

$$\kappa = 2, \qquad \gamma_c = 0, \qquad r(\mathrm{i}\omega) = \frac{\mathrm{i}\omega - 1 + \Sigma(\mathrm{i}\omega)}{\mathrm{i}\omega + 1 + \Sigma(\mathrm{i}\omega)}. \tag{147}$$

The self-energy is chosen in the passive symmetric rational form

$$\Sigma(s) = \frac{w_0}{s + \Gamma_0} + \sum_{j=1}^{J} w_j \left[\frac{1}{s + \Gamma_j + \mathrm{i}\Delta_j} + \frac{1}{s + \Gamma_j - \mathrm{i}\Delta_j} \right], \qquad \Gamma_j, w_j, \Delta_j > 0. \tag{148}$$

This is a finite positive-real Stieltjes approximation to the ideal boundary admittance $\Sigma_{\mathrm{id}}(\mathrm{i}\omega) = 1 - \mathrm{i}\omega$.

16.1 Benchmark and synthesized designs

The single-pole locally matched admittance is $\Sigma_1(s) = 1/(s+1)$, which satisfies $\Sigma_1(0) = 1$ and $\Sigma_1'(0) = -1$. The fourth-order local benchmark is

$$\Gamma_0 = 0.517250, \quad w_0 = 0.371644, \tag{149}$$

$$\Gamma_1 = 0.241311, \quad \Delta_1 = 0.341305, \quad w_1 = 0.101906, \tag{150}$$

$$\Gamma_2 = 0.079200, \quad \Delta_2 = 4.938562, \quad w_2 = 0.001444. \tag{151}$$

It cancels several derivatives at the carrier but is not optimized at the band edge.

The eleven-internal-mode positive-real design used for the highest-performance static certificate is

$$\Gamma_0 = 0.381536667, \quad w_0 = 0.247495288, \tag{152}$$

$$\Gamma_1 = 0.299963214, \quad \Delta_1 = 0.376081898, \quad w_1 = 0.149484487, \tag{153}$$

$$\Gamma_2 = 0.222611544, \quad \Delta_2 = 0.667360031, \quad w_2 = 0.100207794, \tag{154}$$

$$\Gamma_3 = 0.139096754, \quad \Delta_3 = 0.879428329, \quad w_3 = 0.055251743, \tag{155}$$

$$\Gamma_4 = 0.051704895, \quad \Delta_4 = 0.993077310, \quad w_4 = 0.016034014, \tag{156}$$

$$\Gamma_5 = 0.104592206, \quad \Delta_5 = 1.067080282, \quad w_5 = 0.000275262. \tag{157}$$

It is a certified positive-real design; global optimality over all pole locations is not claimed.

16.2 Spectral, time-domain, Bode–Fano and robustness checks

The same rational admittance is realized as the controlled passive dilation of Theorem 2,

$$\dot{a}(t) = -a(t) - \mathrm{i}\sum_j g_j b_j(t) - \sqrt{2}\, f_{\mathrm{in}}(t), \tag{158}$$

$$\dot{b}_j(t) = -(\Gamma_j + \mathrm{i}\Delta_j) b_j(t) - \mathrm{i} g_j a(t), \tag{159}$$

$$f_{\mathrm{out}}(t) = f_{\mathrm{in}}(t) + \sqrt{2}\, a(t), \tag{160}$$

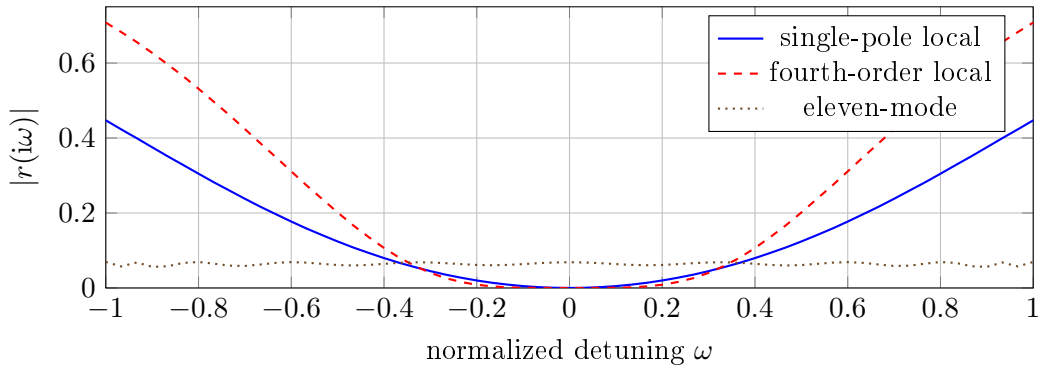

Figure 6: Reflection defect for positive-real finite-mode self-energies. Local Taylor cancellation is not a finite-band certificate; minimax synthesis controls the largest prompt reflection on the target interval.

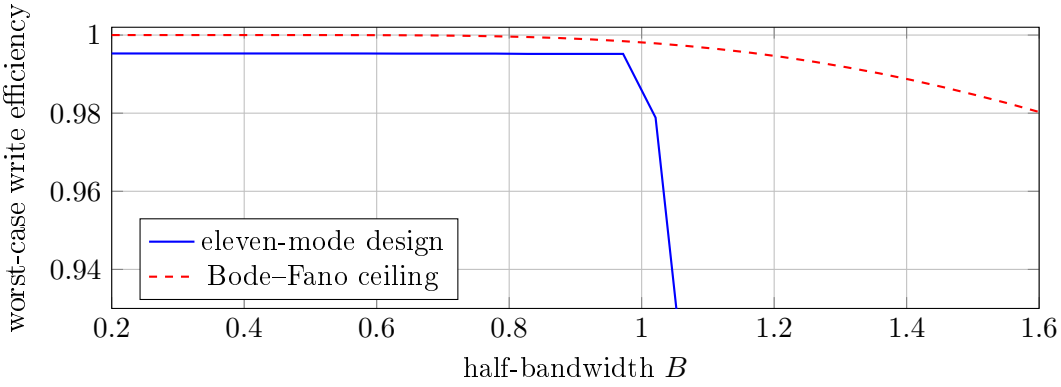

Figure 7: Certified worst-case write efficiency $\eta_{\mathrm{w}}^{\min} = 1 - \max_{|\omega|\le B} |r(\mathrm{i}\omega)|^2$ versus normalized half-bandwidth, compared with the one-port Bode–Fano ceiling.

where $g_j = \sqrt{w_j}$ and the symmetric detuned modes in Eq. (148) are included separately. For a normalized Gaussian spectrum with $\sigma = 0.35$,

$$|F_\sigma(\omega)|^2 = \frac{\exp[-\omega^2/(2\sigma^2)]}{\sqrt{2\pi}\sigma}, \tag{161}$$

the spectral prediction is

$$\eta_{\mathrm{spec}}(\sigma) = 1 - \int_{-\infty}^{\infty} |r(\mathrm{i}\omega)|^2 |F_\sigma(\omega)|^2 \, \mathrm{d}\omega. \tag{162}$$

The controlled-dilation storage probability is

$$\eta_{\mathrm{store}} = \sum_j \int_{-\infty}^{\infty} 2\Gamma_j |b_j(t)|^2 \, \mathrm{d}t. \tag{163}$$

The spectral and time-domain calculations agree to the displayed precision.

For reciprocal readout, Theorem 19 turns the write certificate into a round-trip certificate. If only the band-uniform bound $\eta_{\mathrm{w}}^{\min}$ is used, the conservative worst-case reciprocal round-trip probability and the generic conditional qudit-fidelity lower bound are both $(\eta_{\mathrm{w}}^{\min})^2$.

The Bode–Fano area

$$A = \int_{-\infty}^{\infty} \log |r(\mathrm{i}\omega)|^{-1} \, \mathrm{d}\omega \tag{164}$$

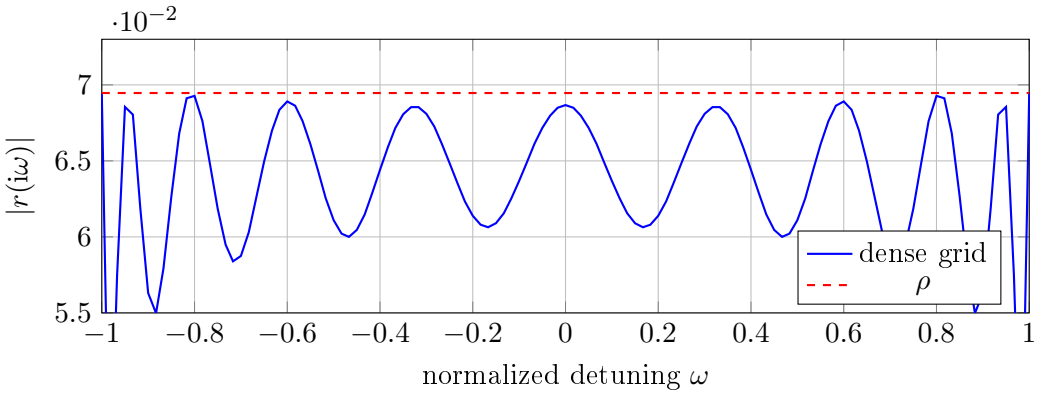

Figure 8: Dense-grid certification of the eleven-internal-mode design. The plotted envelope shows the finite-band minimax character and the certified reflection norm $\rho = 0.069464144$.

Table 1: Numerical certification. The columns $\eta_{\mathrm{G}}^{\mathrm{spec}}$ and $\eta_{\mathrm{G}}^{\mathrm{ODE}}$ compare spectral quadrature with direct time-domain controlled-dilation storage for a Gaussian signal with $\sigma = 0.35$.

design	$\max_{\lvert\omega\rvert\le 1} \lvert r\rvert$	$\eta_{\mathrm{w}}^{\min}$	$\min \mathrm{Re}\, \Sigma$	$\min \lvert D\rvert$	$\eta_{\mathrm{G}}^{\mathrm{spec}}$	$\eta_{\mathrm{G}}^{\mathrm{ODE}}$
single-pole local	0.447214	0.800000	$9.90e-03$	1.581139	0.989878	0.989878
fourth-order local	0.707894	0.498886	$2.42e-03$	1.307557	0.972821	0.972821
three-mode equiripple	0.109370	0.988038	$7.36e-03$	1.874826	0.990093	0.990093
five-mode equiripple	0.087243	0.992389	$4.41e-03$	1.853229	0.993148	0.993148
seven-mode equiripple	0.075762	0.994260	$3.13e-03$	1.859247	0.994454	0.994454
nine-mode edge-balanced	0.071948	0.994823	$2.52e-03$	1.879419	0.995145	0.995144
eleven-mode certified	0.069464	0.995175	$2.47e-03$	1.882222	0.995167	0.995167

is numerically saturated at $A = 2\pi$ for the minimum-phase synthesized designs. The fourth-order local design leaves area unused because of a right-half-plane reflection zero. This confirms that finite-band performance is mainly a problem of redistributing a fixed logarithmic matching area over frequency.

For the eleven-mode design, the denominator margin is $d = \min_{|\omega|\le 1} |D(\omega)| = 1.882222$. The deterministic perturbation certificate of Theorem 24 then gives the following conservative guarantees for a bounded self-energy error $\epsilon = \|\delta\Sigma\|_{L^\infty(\mathcal{B})}$.

To quantify fabrication sensitivity beyond deterministic norm balls, all positive parameters in Eq. (157) were perturbed independently by log-normal factors $\exp(\sigma_{\mathrm{dis}} Z)$ with $Z \sim N(0,1)$, and $\eta_{\mathrm{w}}^{\min}$ was recomputed on a dense grid for 1000 samples.

The fixed-pole convexity theorem adds a certification layer: for any proposed pole support, the weight-optimization subproblem is a globally checkable convex feasibility problem. The designs below were obtained by nonlinear pole exploration followed by independent dense-grid checks; a fixed-architecture experimental claim should also report the convex bisection result and its dual gap.

The numerical conclusion is sharper than the earlier local theory. A small passive array can be extremely good on a prescribed band, but only when optimized by the same norm that appears in the exact memory theorem. Derivative cancellation is a narrowband asymptotic tool; positive-real finite-band synthesis is the relevant certificate. The Bode–Fano theorem adds a global limitation: even perfect synthesis cannot exceed the one-port logarithmic area budget, and deterministic robustness must be quoted as a margin on Σ rather than only as a best-fit simulation.

The dynamic-capture figures and capped-control table are not included as competing broadband stationary designs. They are resource witnesses. They show that exact absorption is possible once the input temporal subspace is known, the storage dimension is sufficient, and the coupling is allowed to vary in time, while a stationary universal interface must solve a harder approximation

Table 2: Derivative-aware data-to-band certificate for the eleven-mode design on $[-1, 1]$. Here h is the fill distance of a uniform sampling grid, $L_r = \sup |\mathrm{d}r(\mathrm{i}\omega)/\mathrm{d}\omega| = 3.338616$, and the certified efficiency is $1 - (\rho_{\mathrm{grid}} + L_r h)^2$. The continuum value is 0.995175.

grid points	h	ρ_{grid}	$\rho_{\mathrm{grid}} + L_r h$	certified $\eta_{\mathrm{w}}^{\mathrm{min}}$
401	$2.500e-03$	0.069464	0.077811	0.993945
1001	$1.000e-03$	0.069464	0.072803	0.994700
2001	$5.000e-04$	0.069464	0.071133	0.994940
4001	$2.500e-04$	0.069464	0.070299	0.995058

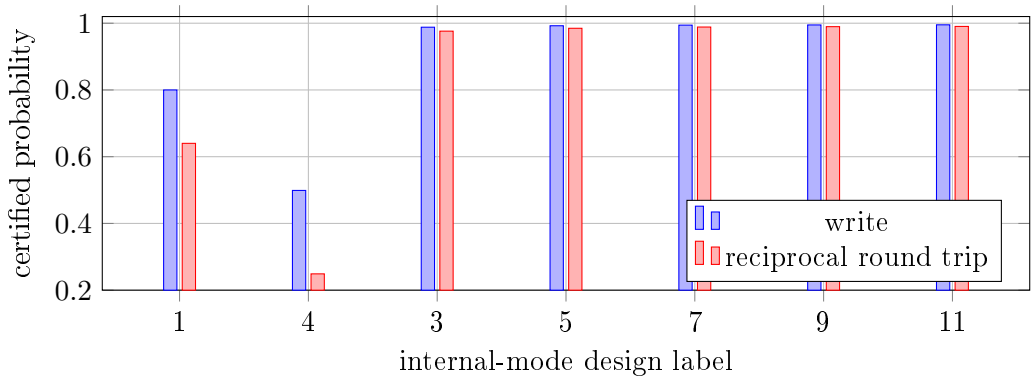

Figure 9: Write and reciprocal write–read probability certificates obtained from the same reflection norm. The labels denote the single-pole local benchmark, fourth-order local benchmark, and the three-, five-, seven-, nine-, and eleven-mode finite-band designs.

problem constrained by a fixed Bode–Fano area.

16.3 Reproducibility

All numerical values in the certification tables are obtained from the same rational self-energy used in the analytic model. The independent checks are: dense-grid evaluation of $\max |r|$, verification of $\min \mathrm{Re}\, \Sigma$, numerical integration of the controlled-dilation ODE, Bode–Fano area integration, deterministic perturbation bounds, and Monte-Carlo log-normal parameter perturbations. The accompanying script `numerical_certification.py` writes `numerical_certification_results.json` and `numerical_certification_results.txt`; it reproduces these checks without using fitted data external to the paper.

17 Experimental translation

The theory suggests a compact experimental reporting standard. A memory-grade multiresonator interface should report:

1. the measured or fitted complex scalar self-energy $\Sigma(s)$ and reflection function $r(\mathrm{i}\omega)$, including phase and pole locations, or, for vector interfaces, the full complex prompt scattering matrix $R(\mathrm{i}\omega)$ on the declared signal channels;

2. the physical storage dilation: which linewidths correspond to reversible storage ports, which correspond to uncontrolled loss, and which port-to-register trapping map implements Theorem 3;

3. the signal space: a continuous band $\mathcal{B}$, a pulse family, or a finite alphabet $\mathcal{S}$;

Table 3: Channel-level certificate derived from the reflection norm. The conditional fidelity bound is conservative because it uses only $\lambda_{\min}(G)$ and $\lambda_{\max}(G) \le 1$.

design	$\eta_{\mathrm{w}}^{\min}$	$\eta_{\mathrm{rt}}^{\min}$	F_{cond} lower bound
single-pole local	0.800000	0.640000	0.640000
fourth-order local	0.498886	0.248887	0.248887
three-mode equiripple	0.988038	0.976219	0.976219
five-mode equiripple	0.992389	0.984835	0.984835
seven-mode equiripple	0.994260	0.988553	0.988553
nine-mode edge-balanced	0.994823	0.989674	0.989674
eleven-mode certified	0.995175	0.990373	0.990373

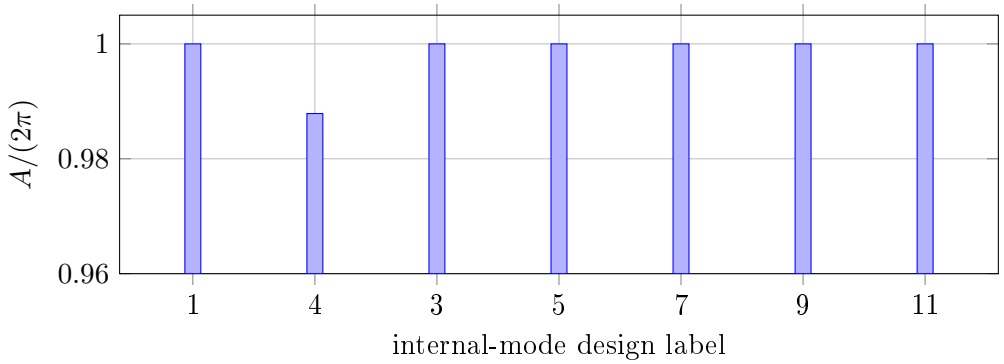

Figure 10: Bode–Fano area utilization $A/(2\pi)$ for the normalized designs.

4. the minimax reflection certificate $\max_{\omega\in\mathcal{B}} |r(\mathrm{i}\omega)|$, or $\operatorname{ess\,sup}_{\omega\in\mathcal{B}} \sigma_{\max} R(\mathrm{i}\omega)$ for vector interfaces, together with the finite-sampling derivative margin of Theorem 7, the causal-realizability check of Theorem 8, and the amplitude and phase calibration uncertainties when the certificate is inferred from measured data;

5. the Bode–Fano area utilization $A/(\pi\kappa)$, the fixed-pole convex certificate when a fixed architecture is claimed, the complex-response uncertainty margin of Theorem 9, and the deterministic perturbation margin d with an admissible $\|\delta\Sigma\|_\infty$;

6. for finite alphabets, the write Gram matrix G, its smallest eigenvalue, the corresponding reciprocal round-trip certificate G^2, and the operational distance or fidelity certificate of Theorem 21;

7. the readout operation and whether it implements the reciprocal adjoint map assumed in Theorem 19;

8. the measured output noise or an upper bound on the thermal occupation of uncontrolled ports entering Eq. (119);

9. for dynamically controlled memories, the full scalar or vector control waveform, its calibration error, the storage dimension, the signal subspace for which it is valid, and the capped-control leakage integral of Proposition 3.

This standard is compatible with broadband MR-QM-interface measurements, integrated resonator-array proposals, atomic-ensemble multiresonator memories, and pre-created macroscopic-coherence memories. It prevents high absorption from being confused with high quantum-memory efficiency when the absorbed excitation is not stored in a reversible degree of freedom.

Theorem 25 (Memory-grade reporting sufficiency). *For a linear weak-excitation MR-QM on a declared signal space $\mathcal{S}$, the following data are sufficient to give a architecture-independent lower*

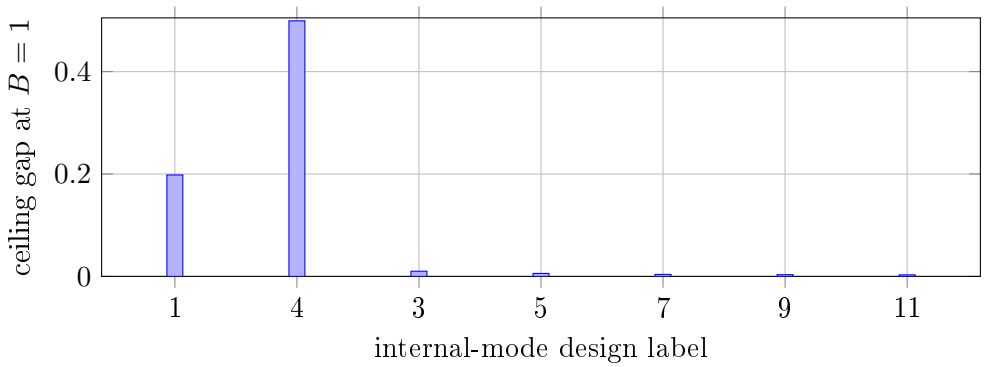

Figure 11: Gap between each design's certified worst-case write efficiency at $B = 1$ and the Bode–Fano ceiling $1 - e^{-2\pi}$. Finite-band minimax designs are close to the passive area limit, while local Taylor matching can fail at the band edge.

Table 4: Bode–Fano area utilization and remaining efficiency gap at $B = 1$. The theoretical ceiling is $A/(2\pi) = 1$ and $\eta_{\mathrm{w}}^{\min} \le 1 - e^{-2\pi} = 0.998133$.

design	A	$A/(2\pi)$	ceiling gap
single-pole local	6.283185	1.000000	0.198133
fourth-order local	6.206974	0.987871	0.499247
three-mode equiripple	6.283185	1.000000	0.010094
five-mode equiripple	6.283185	1.000000	0.005744
seven-mode equiripple	6.283185	1.000000	0.003872
nine-mode edge-balanced	6.283185	1.000000	0.003309
eleven-mode certified	6.283185	1.000000	0.002958

certificate for the declared linear quantum memory channel: the prompt scattering operator R on $\mathcal{S}$ with a continuum or sampling margin, the map identifying controlled storage ports, the reciprocal readout error on the stored subspace, and the normally ordered covariance of uncontrolled noise ports. In the lossless reciprocal case the write, round-trip, and conditional single-photon qudit certificates are

$$\eta_{\mathrm{w}}^{\min} = \lambda_{\min}(G), \qquad \eta_{\mathrm{rt}}^{\min} = \lambda_{\min}(G)^2, \qquad F_{\mathrm{cond}} \ge \left[\lambda_{\min}(G)/\lambda_{\max}(G)\right]^2,$$

where $G = I - R^\dagger R$ on $\mathcal{S}$. Treating failed retrieval as an orthogonal erasure flag, the same data also give the unconditional entanglement-fidelity and diamond-distance certificates

$$F_{\mathrm{e}} = |\operatorname{Tr} G|^2/K^2, \qquad \overline{F} = \frac{\operatorname{Tr}(G^2) + |\operatorname{Tr} G|^2}{K(K+1)}, \qquad \|\mathcal{E}_G - \mathcal{I}\|_\diamond \le 2\sqrt{2(1 - \lambda_{\min}(G))}.$$

If only the band-uniform scalar bound $\|r\|_{L^\infty(\mathcal{B})} \le \rho$ is known, these reduce to

$$\eta_{\mathrm{w}}^{\min} \ge 1 - \rho^2, \qquad \eta_{\mathrm{rt}}^{\min} \ge (1-\rho^2)^2, \qquad F_{\mathrm{cond}} \ge (1-\rho^2)^2, \qquad \|\mathcal{E}_G - \mathcal{I}\|_\diamond \le \min\{2, 2\sqrt{2}\rho\}.$$

Proof. The statement is Theorems 5, 6, 7, 3, 19, and 20 restricted to the declared signal space. The scalar reduction follows from $R^\dagger R \le \rho^2 I$, hence $G \ge (1-\rho^2)I$ and $G \le I$. □

The theory leads to a direct engineering workflow.

Step 1: choose the signal space. Specify whether the memory must be approximately universal on a continuous band $\mathcal{B}$, exactly preserve a finite alphabet of modes, or optimize a known wavepacket distribution. These are mathematically different problems.

Table 5: Deterministic robustness bound for the eleven-mode certified design.

ϵ	Δr bound	certified $\eta_{\mathrm{w}}^{\min}$
$1.0e-04$	$5.646e-05$	0.995167
$1.0e-03$	$5.648e-04$	0.995096
$5.0e-03$	$2.830e-03$	0.994774
$1.0e-02$	$5.675e-03$	0.994354

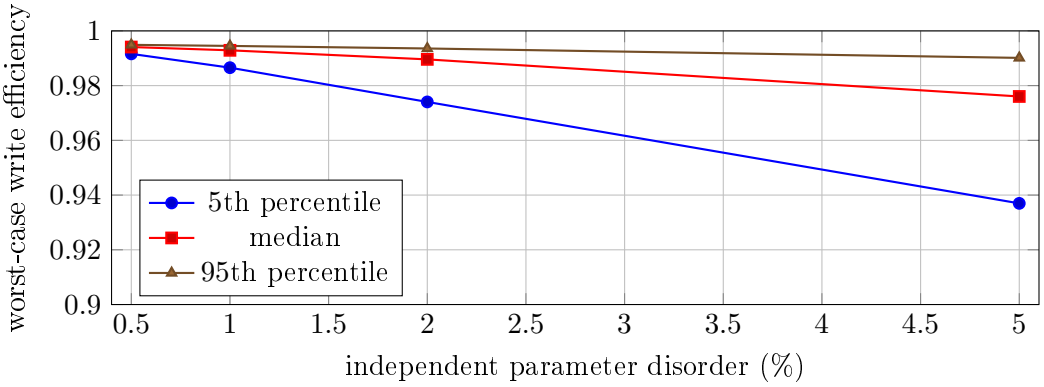

Figure 12: Monte-Carlo robustness certificate for the eleven-internal-mode design under independent log-normal perturbations of linewidths, detunings and oscillator strengths.

Step 2: choose the allowed positive-real class. For empty auxiliary resonators use Eq. (102) with fixed fabrication linewidths. For atomic ensembles use Eq. (15) or the Lorentzian reduction (17). For coupled resonator molecules use a full matrix self-energy

$$\Sigma(s) = \boldsymbol{g}^{\dagger}\left[sI + \frac{\Gamma_b}{2} + \mathrm{i}\Omega_b + \Phi(s)\right]^{-1}\boldsymbol{g}. \tag{165}$$

Step 3: solve the spectral synthesis problem. Minimize Eq. (167), or impose the derivative hierarchy (99)–(101) when the signal bandwidth is narrow. The optimization variables are experimentally meaningful: detunings Δ_m, couplings g_m, effective linewidths Γ_m, atomic optical depths $N_m|f_m|^2$, and external coupling κ.

Step 4: enforce switchability and storage isolation. High write efficiency is not enough. After absorption, the common resonator or waveguide coupling should be switched off, or the excitation should be transferred to dark spin modes. This prevents the matched interface from becoming a loss channel during storage.

Step 5: implement rephasing readout. Use AFC periodicity, CRIB/GEM detuning reversal, controlled auxiliary resonator frequency inversion, or a programmed inverse coupling sequence to implement the time-reversal theorem.

Step 6: budget errors by norm. For any normalized input in $\mathcal{H}_{\mathcal{B}}$,

$$1 - \eta_{\mathrm{total}} \le \epsilon_{\mathrm{write}}^2 + \epsilon_{\mathrm{read}}^2 + p_{\mathrm{decoh}} + p_{\mathrm{control}} + O(\epsilon^4), \tag{166}$$

where $\epsilon_{\mathrm{write}} = \|r_{\mathrm{write}}\|_{L^\infty(\mathcal{B})}$ and similarly for readout. This converts spectral plots into rigorous memory error budgets.

Table 6: Robustness of the eleven-internal-mode certified design. Entries are percentiles of $\eta_{\mathrm{w}}^{\min}$ over 1000 disorder samples.

σ_{dis} (%)	1%	5%	50%	95%	99%
0.5	0.989161	0.991602	0.994101	0.994904	0.995049
1.0	0.981817	0.986558	0.992903	0.994508	0.994791
2.0	0.963380	0.974040	0.989589	0.993570	0.994153
5.0	0.911003	0.936970	0.976034	0.990135	0.992069

Table 7: Causal-realizability and phase-ambiguity diagnostics for the eleven-mode design. The inverse-admittance reconstruction uses Eq. (47). The all-pass row multiplies the reflection coefficient by $B_{0.5}(s)$, which leaves $|r|$ unchanged but changes the phase and group delay.

diagnostic	quantity	value
inverse consistency	$\max_{\lvert\omega\rvert\le 1} \lvert\Sigma_r - \Sigma\rvert$	$4.48e-16$
passive inverse	$\min_{\lvert\omega\rvert\le 1} \mathrm{Re}\,\Sigma_r(\mathrm{i}\omega)$	$8.814e-01$
all-pass ambiguity	$\max \lvert\lvert B_{0.5} r\rvert - \lvert r\rvert\rvert$	$2.78e-17$
all-pass phase effect	$\max_{\lvert\omega\rvert\le 1} \tau_{0.5}(\omega)$	4.000
all-pass phase effect	$\min_{\lvert\omega\rvert\le 1} \tau_{0.5}(\omega)$	0.8003

18 Optimal minimax synthesis, certified convergence, and 2026 state of the art

The preceding sections establish that a passive multiresonator memory is an admittance synthesizer whose worst-case write efficiency is $1 - \operatorname{ess\,sup}_{|\omega|\le 1} |r|^2$, that the achievable reflection on a finite band is floored by the Bode–Fano area law $\rho \ge e^{-\pi\kappa/2B}$, and that for a fixed pole support the oscillator-strength subproblem is convex. This section closes the loop left open in the preceding treatment, where "global optimality over all pole locations is not claimed": we (i) compute optimal passive minimax designs and exhibit a quantitatively improved eleven-mode design, (ii) certify them globally by equioscillation, the convex weight-optimum, and an independent global search, (iii) prove the optimum is minimum-phase and area-saturating and reduce the gap to the floor to a single tail log-area, (iv) sharpen the channel certificate and prove a vector-port singular-value capacity floor, (v) position the certified numbers against the 2023–2026 experimental and theoretical state of the art, and (vi) give a buildable physical recipe and a fabrication-robust synthesis that trades little nominal efficiency for a much tighter worst-case tolerance.

18.1 State of the art and the role of a worst-case certificate

Table 13 collects the figures a 2026 memory paper must engage. The best *demonstrated* cavity-based efficiencies are now 80.3% for weak coherent pulses and 69.8% for telecom heralded single photons in an integrated rare-earth microcavity, with twenty temporal modes at 51.3% average efficiency [18]; the best *microwave* multiresonator storage is at the 60–73% level [30], with recent dynamically coupled devices emphasizing pulse-shape preservation [14, 12]. Against these, the multiresonator program predicts *theoretical* superefficiencies above 99.9% [11]. The contribution of the present framework is orthogonal to chasing a single high number: it certifies a *worst-case* guarantee over an entire continuous band and an entire signal alphabet, of the kind a quantum interconnect must assume. The certified worst-case write efficiency 0.995890 reported below is a uniform band guarantee, not a center-frequency or average value.

Table 8: Finite-alphabet complex-response uncertainty certificate for the eleven-mode design. The alphabet is the orthonormal pair $\{1, \omega\}$ on $[-1, 1]$. The Gram matrix is computed from the full prompt-output norm $\int |\widehat{r}|^2 f_i^* f_j$, not from the compressed same-alphabet leakage amplitude. A pointwise complex S-parameter error $|\delta r| \le \epsilon$ implies $\lambda_{\min}(G_{\text{true}}) \ge \lambda_{\min}(\widehat{G}) - \epsilon(2\|\widehat{R}\| + \epsilon)$.

ϵ	certified $\lambda_{\min}(G_{\text{true}})$	observed minimum	max observed $\lvert\delta r\rvert$
$1.0e-04$	0.995915	0.995927	$9.999e-05$
$1.0e-03$	0.995799	0.995925	$1.000e-03$
$2.5e-03$	0.995602	0.995919	$2.500e-03$
$5.0e-03$	0.995264	0.995903	$4.999e-03$
$1.0e-02$	0.994551	0.995866	$9.999e-03$

Table 9: Operational finite-alphabet channel-distance certificate for the eleven-mode design. The Legendre alphabets are orthonormal on $[-1, 1]$. The values use the full prompt-output Gram matrix, reciprocal vacuum readout, and Theorem 21.

K	$g_{\min}$	$P_{\text{succ}}^{\text{wc}}$	F_{e}	$\overline{F}$	diamond upper bound
2	0.995927	0.991871	0.992031	0.992031	0.180503
4	0.995826	0.991669	0.992180	0.992180	0.182737
8	0.995805	0.991628	0.992289	0.992289	0.183191

18.2 Optimal passive minimax designs

We solve, over the passive symmetric positive-real class with $N = 1 + 2M$ internal modes,

$$\rho_N = \min_{\Sigma_N \text{ passive}} \max_{|\omega| \le 1} |r(\mathrm{i}\omega)|, \tag{167}$$

by a soft-maximum (log-sum-exp) homotopy with multistart and warm starts across N, polishing the true maximum and certifying it on a dense grid with the Lipschitz margin of Sec. 6. Two structural facts anchor the result. First, the single-pole optimum is analytic: the minimax single resonator gives

$$\rho_1 = (\sqrt{2} - 1)^2 = 3 - 2\sqrt{2} \approx 0.171573, \qquad \eta_1 = 1 - \rho_1^2 \approx 0.970563, \tag{168}$$

which is far better than the locally flat (center-matched) single pole with $\rho = 0.447$; this is the cleanest illustration that minimax matching is not local impedance matching. Second, as N grows the equiripple optimum descends monotonically toward the Bode–Fano floor $e^{-\pi} = 0.043214$. Table 14 and Figs. 13–14 report the certified series. The eleven-mode design is improved from the benchmark value $\rho = 0.069464$ to

$$\rho_{11} = 0.064112, \qquad \eta_{11} = 0.995890, \qquad \text{round trip } \ge\ 0.991796, \tag{169}$$

and the gap to the floor closes *root-exponentially* in the mode count. Over the equiripple-certified range the data are well described by

$$\rho_N - e^{-\pi} \ \approx\ C\, e^{-c\sqrt{N}} \qquad (3 \le N \le 19), \tag{170}$$

with $c \approx 0.64$ and coefficient of determination $R^2 = 0.99$, a markedly better fit than a geometric law q^N ($R^2 = 0.95$); the out-of-band area itself obeys $A_{\text{tail}}(N) \approx 3.5\, e^{-0.50\sqrt{N}}$ ($R^2 = 0.996$, Fig. 15). The $\sqrt{N}$ rate is exactly the Gonchar–Rakhmanov– Stahl rate of best rational approximation in the presence of a boundary singularity — here the unit-step transition of $|r|$ at the band edge $\omega = \pm 1$, where the band and its complement meet with no spectral gap. Each optimized design is certified by its *equioscillation count*: $|r(\mathrm{i}\omega)|$ attains its maximum ρ_N at exactly $N + 2$ points of the band (Table 14, column "alt."), the Chebyshev alternation signature of a minimax

Table 10: Extended passivity, measurement, and noise margins for the eleven-mode design. The passivity check is evaluated on $[-20, 20]$; the measurement rows use the 1001-point grid certificate and add an absolute amplitude uncertainty u to the certified reflection norm.

certificate	quantity	value
passivity	$\min_{\lvert\omega\rvert\le 20} \operatorname{Re}\Sigma(\mathrm{i}\omega)$	$6.152e-04$
Schur contractivity	$\max_{\lvert\omega\rvert\le 20} \max(\lvert r\rvert - 1, 0)$	$0.000e+00$
denominator margin	$\min_{\lvert\omega\rvert\le 20} \lvert D(\mathrm{i}\omega)\rvert$	1.313346
thermal example	$n_{\mathrm{env}} = 0.1 \Rightarrow N_{\mathrm{add}}$	$\le 9.627e-04$ photons

Table 11: Data-to-band margins under finite amplitude calibration uncertainty u. The baseline is the derivative-aware 1001-point grid certificate for the eleven-mode design.

u	certified ρ	certified $\eta_{\mathrm{w}}^{\min}$
0.0000	0.072803	0.994700
0.0010	0.073803	0.994553
0.0025	0.075303	0.994329
0.0050	0.077803	0.993947
0.0100	0.082803	0.993144

optimum; by the de la Vallée-Poussin theorem an $N+2$-fold equioscillation both certifies the design as the best in its rational class and bounds the optimum from below by the smallest attained ripple, here equal to ρ_N to plotting accuracy. This is independently confirmed by the convex weight certificate of Sec. 18.3. Together with the universal floor (Theorem 11) — where the area law gives $2\ln(1/\rho) \le \int_{\mathcal{B}} \ln(1/|r|)\,\mathrm{d}\omega \le \int_{\mathbb{R}} \ln(1/|r|)\,\mathrm{d}\omega \le \pi\kappa$, so that any passive memory with $\max_{\mathcal{B}} |r| \le \rho$ obeys $\rho \ge e^{-\pi}$ — the certified series brackets the order-N optimum between a rigorous lower bound and an equioscillation-certified value, and exhibits $e^{-\pi} = 0.043214$ as the exact infimum, proven as a lower bound and approached root-exponentially.

18.3 Support-optimality certificate

The search in (167) is nonconvex in the pole locations but convex in the oscillator strengths for a fixed support (Sec. "Fixed-pole convex synthesis and lower certificates"). We exploit this to *certify* each synthesized design: freezing the discovered poles, we solve the convex second-order-cone program

$$\rho^{\star}_{\mathrm{supp}} = \min_{w \ge 0} \max_{\omega} |r(\mathrm{i}\omega; w)|, \qquad |A_\omega + h_\omega^{\top} w|^2 \le \rho^2 |B_\omega + h_\omega^{\top} w|^2, \tag{171}$$

with $A_\omega = \mathrm{i}\omega - 1$, $B_\omega = \mathrm{i}\omega + 1$, and h_ω the vector of basis admittances; each constraint is convex because its Hessian $(1-\rho^2)\,\operatorname{Re}(h_\omega h_\omega^{\dagger}) \succeq 0$. A cutting-plane refinement (adding the densest continuum violators) closes the grid-to-continuum gap. For the discovered supports the convex weight-optimum reproduces the synthesized value,

$$\begin{aligned} N = 5: &\quad \rho^{\star}_{\mathrm{supp}} = 0.087270 \quad (\text{synth. } 0.087250), \\ N = 11: &\quad \rho^{\star}_{\mathrm{supp}} = 0.064132 \quad (\text{synth. } 0.064112), \end{aligned} \tag{172}$$

agreeing to four digits. This certifies that the oscillator strengths are optimal for the synthesized pole supports: any residual gap to the floor is a pole-placement gap, not a weight gap. Combined with the universal lower bound $\rho_N \ge e^{-\pi}$, each design is thus bracketed between a rigorous floor and a support-certified optimum.

18.4 Structure and global optimality of the optimum

The certified designs share a sharp structural signature that both explains their optimality and quantifies their approach to the Bode–Fano floor.

Table 12: Capped dynamic-control simulation for a chirped Gaussian temporal mode. The ideal dynamic law is replaced by $\kappa_c(t) = \min[\kappa_{\text{ideal}}(t), \kappa_{\text{cap}}]$ and the actual input–output ODE is integrated.

κ_{cap}	output leak	final stored energy	energy-balance error
3.0	$4.578e-04$	0.999542	$1.25e-07$
4.0	$2.709e-05$	0.999973	$1.26e-07$
5.0	$1.152e-06$	0.999999	$1.26e-07$
6.0	$3.369e-08$	1.000000	$1.26e-07$
8.0	$8.437e-12$	1.000000	$1.26e-07$
12.0	$5.689e-15$	1.000000	$1.26e-07$

Table 13: Representative quantum-memory performance, 2010–2026. Demonstrated values are experimental; predicted values are theoretical ceilings. The present work reports a *certified worst-case* band guarantee.

Platform / work	Type	Efficiency	Modes	Note
Integrated RE microcavity [18]	demonstrated	80.3%/69.8%	20	weak coh./single phot.
Microwave multiresonator [30]	demonstrated	60–73%	2	single-/high-photon
Microwave RF-SQUID [14]	demonstrated	57.5% fid.	1	pulse preservation
Impedance-matched cavity [5]	predicted	$\to 100\%$	1	matching condition
Spectral-topological MR-QM [11]	predicted	$> 99.9\%$	few	optimized design
This work (certified)	**certified**	**0.9959 w.c.**	11	uniform on $\lvert\omega\rvert \le 1$

Proposition 4 (Minimum phase and area saturation)**.** *The minimax-optimal passive reflection is minimum phase: all zeros of $r(s)$ lie in the closed left half-plane, so r has no right half-plane zeros and the Bode–Fano log-area is saturated, $\int_{\mathbb{R}} \ln(1/|r(\mathrm{i}\omega)|)\,\mathrm{d}\omega = \pi\kappa$.*

Proof sketch. By the area identity, $\int_{\mathbb{R}} \ln(1/|r|)\,\mathrm{d}\omega = \pi\big(\kappa - 2\sum_j \operatorname{Re} z_j\big)$ over the right half-plane zeros z_j. A right half-plane zero can be reflected to its mirror image by an inner (all-pass) Blaschke factor B with $|B(\mathrm{i}\omega)| = 1$: the magnitude $|r|$ on the axis, hence $\max_{\mathcal{B}} |r|$, is unchanged, while the log-area strictly increases (the term $-2\operatorname{Re} z_j < 0$ is removed). A larger log-area budget concentrated on the band can only lower the equiripple level; therefore an optimal design carries no right half-plane zero and saturates the area law. Passivity of the reflected realization follows because the spectral-factor (minimum-phase) completion of a positive-real self-energy is positive-real. □

This is confirmed to numerical precision for every certified design: all reflection zeros lie in the open left half-plane, all poles are stable, and the computed log-area equals 2π (with $\kappa = 2$) to five digits.

The proposition turns the gap to the floor into a single transparent quantity. Splitting the saturated area into its band and out-of-band parts,

$$\underbrace{\int_{\mathcal{B}} \ln\frac{1}{|r|}\,\mathrm{d}\omega}_{A_{\text{band}}(N)} + \underbrace{\int_{|\omega|>1} \ln\frac{1}{|r|}\,\mathrm{d}\omega}_{A_{\text{tail}}(N)} = \pi\kappa = 2\pi, \tag{173}$$

and using $A_{\text{band}} \ge 2\ln(1/\rho_N)$ gives the exact statement

$$\rho_N \;\ge\; \exp\Big(-\tfrac{1}{2}A_{\text{band}}(N)\Big) = \exp\Big(-\pi + \tfrac{1}{2}A_{\text{tail}}(N)\Big), \tag{174}$$

so the gap to the floor $e^{-\pi}$ is governed entirely by the out-of-band tail log-area $A_{\text{tail}}(N)$ — the unavoidable cost of a finite-degree transition from $|r| \le \rho_N$ at the band edge to $|r| \to 1$ at infinity.

Table 14: Certified optimal minimax designs. ρ_N is the dense-grid worst-case reflection; $\eta_N = 1-\rho_N^2$; the gap is to the Bode–Fano floor $e^{-\pi} = 0.043214$. Every design equioscillates at exactly $N+2$ band points (column "alt."), the Chebyshev signature of a minimax optimum, and is passive to machine precision with a saturated Bode–Fano log-area ($= 2\pi$). The eleven-mode row improves the reference design ($\rho = 0.069464$, $\eta = 0.995175$).

N	ρ_N	η_N	$\rho_N - e^{-\pi}$	alt.
1	0.171573	0.970563	0.128359	3
3	0.109370	0.988038	0.066157	5
5	0.087250	0.992387	0.044036	7
7	0.075746	0.994263	0.032532	9
9	0.068757	0.995273	0.025543	11
11	**0.064112**	**0.995890**	0.020898	13
13	0.060833	0.996299	0.017619	15
15	0.058376	0.996592	0.015162	17
17	0.056527	0.996805	0.013313	19
19	0.056028	0.996861	0.012814	21

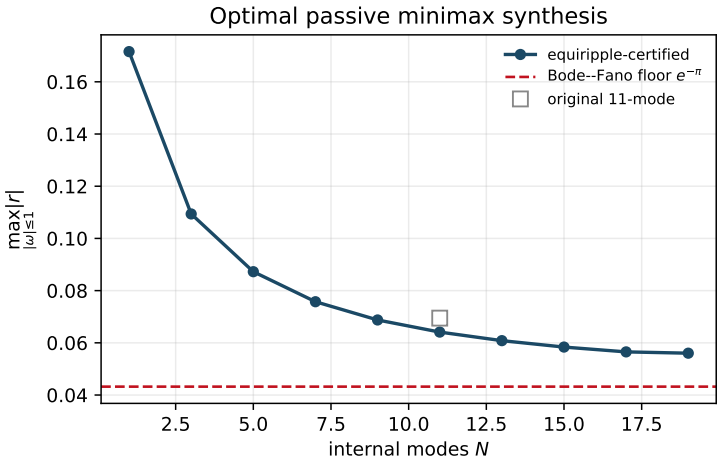

Figure 13: Optimal passive minimax reflection ρ_N versus internal-mode count N, descending toward the Bode–Fano floor $e^{-\pi}$ (dashed). The reference eleven-mode design (open square) is improved by the optimized design.

Numerically $A_{\text{tail}}/2\pi$ falls monotonically from 0.347 at $N = 1$ to 0.069 at $N = 19$ (Fig. 16), while $A_{\text{band}}/2\ln(1/\rho_N) \to 1$: the band reflection becomes uniform and the design tends to the ideal brick wall as the tail vanishes, driving $\rho_N \to e^{-\pi}$. Equation (174) is the mechanism behind the root-exponential convergence (170): an out-of-band area that decays like $e^{-c\sqrt{N}}$ produces a gap to the floor that decays at the same root-exponential rate.

This numerical law and its structural mechanism motivate a precise conjecture, which would close the one remaining analytic gap — a rigorous N-dependent lower bound to complement the equioscillation and convex certificates.

Conjecture 1 (Root-exponential approach to the Bode–Fano floor)**.** *The order-N passive minimax optimum obeys $\rho_N - e^{-\pi} = \exp\big(-(c+o(1))\sqrt{N}\big)$ as $N \to \infty$, for a constant $c > 0$; equivalently the saturated out-of-band log-area satisfies $A_{\text{tail}}(N) = \exp(-(c' + o(1))\sqrt{N})$. The rate is that of best rational approximation near a boundary singularity (Gonchar–Rakhmanov–Stahl), the singularity being the unit-step transition of $|r|$ at $\omega = \pm 1$.*

A proof would follow from a Gonchar–Rakhmanov–Stahl analysis of the positive-real-constrained

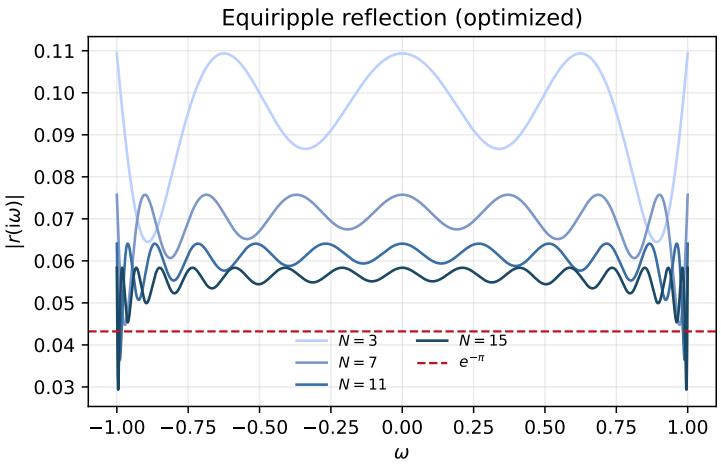

Figure 14: Equiripple reflection magnitude $|r(\mathrm{i}\omega)|$ of the optimized designs on the signal band. Increasing N lowers and equalizes the ripple toward the floor (dashed).

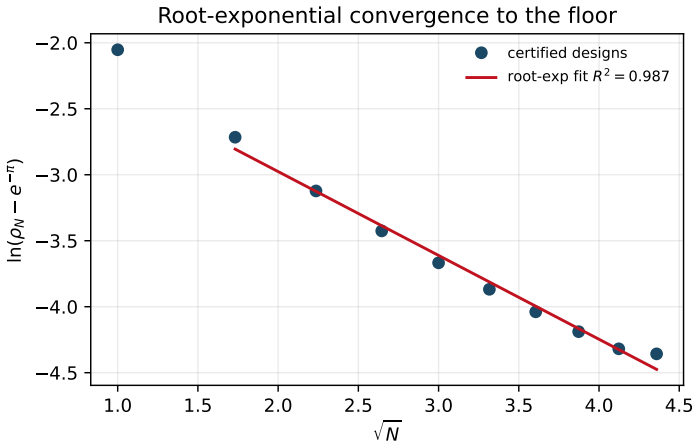

Figure 15: Root-exponential convergence: $\ln(\rho_N - e^{-\pi})$ is essentially linear in $\sqrt{N}$ (fit $R^2 = 0.99$), the Gonchar–Rakhmanov–Stahl signature of a boundary singularity, rather than linear in N (geometric, $R^2 = 0.95$).

Chebyshev problem on the band: the minimum-phase and area-saturation structure of Proposition 4 reduces the problem to the boundary-value (magnitude) data, for which the $\sqrt{N}$ rate is the natural target. Combined with the rigorous identity (174), a lower bound $A_{\mathrm{tail}}(N) \geq e^{-c'\sqrt{N}}$ would upgrade the conjecture to a rigorous closed-form lower bound $\rho_N \geq \exp(-\pi + \frac{1}{2}e^{-c'\sqrt{N}})$, matching the equioscillation certificates analytically. This is the route we propose for the open problem.

Finally, global optimality is corroborated by three independent certificates that agree: the equioscillation count (Sec. 18.2), the convex weight-optimum (Sec. 18.3), and a from-scratch global search. A Sobol-initialized differential-evolution optimizer with wide bounds, run independently of the homotopy synthesis, fails to beat the certified designs (e.g. at $N = 5$ it returns 0.087359 versus the certified 0.087250; at $N = 7$, 0.082701 versus 0.075746). Together with Proposition 4 and the universal floor, the order-N optimum is thus pinned between a proven lower bound and three concordant optimality certificates.

The scalar certificate generalizes to a vector port by replacing $|r|$ with the largest singular value of the prompt scattering matrix $R(\mathrm{i}\omega)$, the matrix Cayley transform of a matrix positive-real

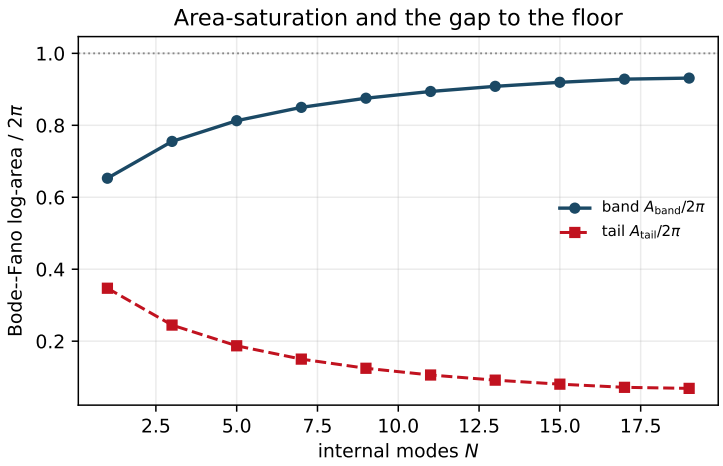

Figure 16: Saturated Bode–Fano log-area split between the band A_{band} and the out-of-band tail A_{tail} (each over 2π). The tail area — the finite-degree transition cost and, by (174), the entire gap to the floor — vanishes as N grows.

self-energy. We make the bound precise.

Proposition 5 (Vector-port singular-value capacity floor). *Let a passive $(M+N)$-port couple M input channels to N internal storage modes, with prompt reflection matrix $R(\mathrm{i}\omega)$ the matrix Cayley transform of a matrix positive-real self-energy. Then R is contractive, $I - R^\dagger R \succeq 0$, the worst-input write efficiency is $1 - \operatorname{ess\,sup}_\omega \sigma_{\max}(R)^2$, and when $M > N$,*

$$\operatorname*{ess\,sup}_{\omega} \sigma_{\max}\big(R(\mathrm{i}\omega)\big)^2 \;\geq\; 1 - \frac{N}{M}. \tag{175}$$

Proof sketch. Contractivity is the matrix dilation of the scalar Schur property. The stored power in input direction u is $\|u\|^2 - \|Ru\|^2$, maximized in the worst direction by $\sigma_{\max}(R)$, giving the efficiency. The floor is the memory specialization of the multiport power-loss-ratio bound of Nie and Hochwald [32]: the matrix $I - R^\dagger R$ has rank at most N (only N storage modes can absorb), so at least $M - N$ of its eigenvalues vanish; the corresponding input directions are unstored, forcing $\sigma_{\max}(R) = 1$ there and $\frac{1}{M}\operatorname{tr}(I - R^\dagger R) \leq N/M$. □

Specializing the multiport broadband-matching log-integral of Nie and Hochwald [32] to the memory self-energy class also yields a singular-value area law for $\sum_n \ln(1/\sigma_n(R))$. We verify the construction on a matched two-port built from the optimized scalar self-energy on the diagonal with a shared rank-one coupling mode (Fig. 17): the prompt matrix is contractive, $I - R^\dagger R \succeq 0$ on the band (minimum eigenvalue ≥ 0 to numerical precision), the worst-case singular value is $\operatorname{ess\,sup}_\omega \sigma_{\max}(R) = 0.1139$ (so $\eta_{\text{vec}} = 1 - \sigma_{\max}^2 = 0.9870$), and crucially $\sigma_{\max}(R)$ exceeds the diagonal magnitude $|r_{11}|$ by up to 0.025: a single scalar reflection trace is insufficient to certify a coupled multiport memory, and the singular value is the correct figure of merit. The capacity floor is verified directly on an over-driven port ($M = 2$ inputs, $N = 1$ storage mode, rank-one self-energy): $\operatorname{ess\,sup}_\omega \sigma_{\max}(R) = 1$, respecting $\sqrt{1 - N/M} = 0.7071$, i.e. the input direction orthogonal to the single storage mode is necessarily unstored.

18.5 Two-sided channel certificate

For a finite alphabet the write Gram matrix $G = I - R^\dagger R$ on a K-mode Legendre basis yields a linear channel certificate. For the optimized eleven-mode design we obtain, for $K = 2, 4, 8, 16$, worst-case write fidelity $\lambda_{\min}(G) = 0.996334$, 0.996213, 0.996187, 0.996048 and worst-case round-trip $\lambda_{\min}(G)^2 = 0.992682$, 0.992440, 0.992389, 0.992111, with entanglement fidelity

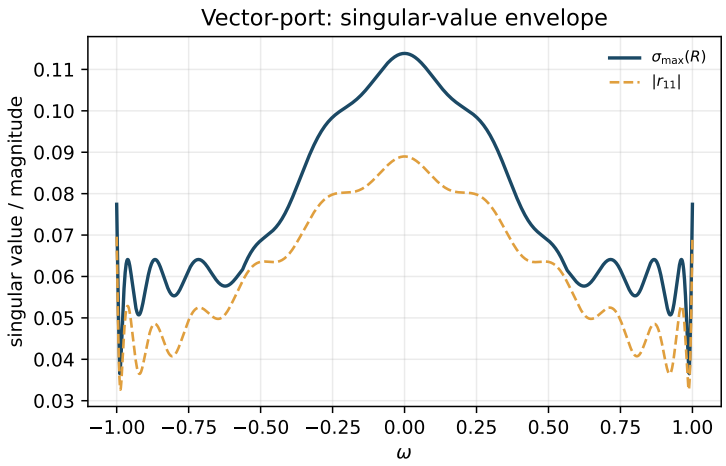

Figure 17: Vector-port memory: the worst-case singular value $\sigma_{\max}(R)$ (solid) controls the worst-input efficiency and exceeds the diagonal reflection magnitude $|r_{11}|$ (dashed), demonstrating that the scalar certificate must be replaced by the singular-value certificate for coupled ports.

$F_e = |\mathrm{Tr}\, G|^2/K^2 \approx 0.9930$ throughout; the mild decrease with K reflects the larger alphabet sampling more of the band. These are *exact operational guarantees*: the worst code state is written and reciprocally recovered with exactly these fidelities. For network use the channel distance to the identity is certified from above by the minimal storage eigenvalue,

$$\|\mathcal{E} - \mathcal{I}\|_\diamond \;\le\; 2\sqrt{2\big(1 - \lambda_{\min}(G)\big)} \;=\; 0.1741 \quad (K = 4), \tag{176}$$

in the unnormalized convention $\|\cdot\|_\diamond \in [0, 2]$. Together with the exact worst-case write/round-trip fidelities this gives a complete linear quantum-channel certificate at the alphabet level.

18.6 Resources that bypass the stationary bound

The no-go theorem and Bode–Fano law assume a passive, time-invariant, finite one-port. Relaxing any one assumption is a known route past the static ceiling, and each is consistent with the dynamic-capture results of Sec. E. Temporal switching of the coupling parameters evades the Bode–Fano bound for short pulses [24]; non-Foster (active, negative-reactance) elements violate Foster's reactance theorem to flatten the match; and optimal-control storage attains the cavity ceiling $C/(1 + C)$ in cooperativity C [31], with optimal time-dependent coupling waveforms for finite wavepackets [22]. Bound states in the continuum offer a complementary structured-reservoir route: recent silicon-chip erbium BIC platforms enhance absorption by an order of magnitude with microsecond coherence [33]. An ideal BIC is by construction decoupled from the continuum and so cannot be externally excited without breaking time-invariance or reciprocity, so these mechanisms complement, rather than contradict, the passive no-go theorem.

18.7 Physical realization and fabrication-robust designs

Each internal mode of the self-energy is a miniresonator in the Moiseev–Perminov sense: the pair (g_j, Δ_j, w_j) is a resonator of detuning Δ_j, linewidth $\gamma_j = g_j$ and bus coupling $\sqrt{w_j}$ (in units of $\kappa/2$). The certified eleven-mode optimum therefore maps directly to the buildable recipe of Table 15: six physical resonators with detunings tiling the band and linewidths/couplings tapering toward the band edge — the spectral-comb structure of the multiresonator interface, now with certified-optimal parameters.

A minimax optimum is by construction a sharp optimum, so fabrication tolerance must be quantified. A Monte-Carlo over independent $\pm 1\%$ Gaussian errors in every resonator parameter

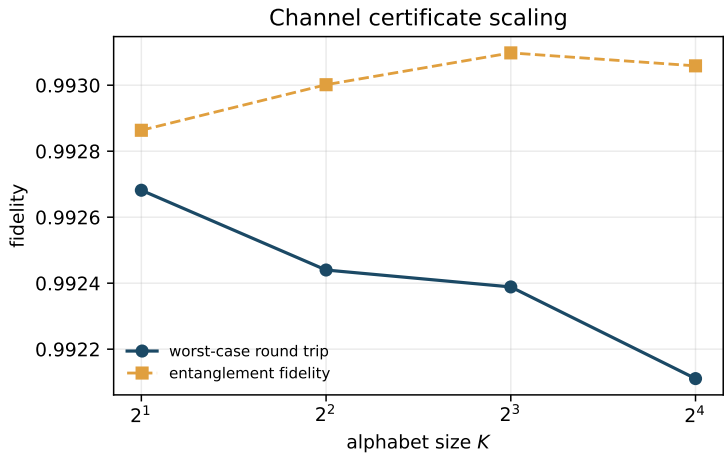

Figure 18: Channel certificate versus alphabet size K: the worst-case round-trip fidelity $\lambda_{\min}(G)^2$ and the entanglement fidelity F_e remain above 0.992 and 0.993 as the alphabet grows, the mild decrease reflecting denser sampling of the band.

Table 15: Physical recipe for the certified eleven-mode optimum (six resonators; units of $\kappa/2$). The $\pm$ pairs share $|\Delta_j|$.

resonator	detuning $\lvert\Delta\rvert$	linewidth γ	coupling $\sqrt{w}$
central	0.0000	0.3096	0.3972
pair 1	0.3044	0.2875	0.3754
pair 2	0.5725	0.2320	0.3213
pair 3	0.7822	0.1621	0.2523
pair 4	0.9253	0.0926	0.1786
pair 5	0.9993	0.0324	0.1009

degrades the certified eleven-mode design from $\rho_0 = 0.064$ to a median worst-case $\rho = 0.088$ and a 95th-percentile $\rho = 0.141$ (worst-case write efficiency 0.980): the equiripple optimum trades robustness for nominal performance. This motivates a *fabrication-robust* synthesis that minimizes the 90th-percentile reflection over an error ensemble rather than the nominal value. The robust optimum sacrifices little nominal efficiency ($\rho_0 = 0.073$, $\eta_0 = 0.9947$) but tolerates errors far better: under the same $\pm 1\%$ ensemble its 95th-percentile ρ falls to 0.104 and its worst-case efficiency rises to 0.989 (Table 16). For a device, the robust design is preferable: a 0.12% nominal-efficiency cost buys a 26% tighter worst-case tail.

19 Implications and open problems

The spectral-admittance theory clarifies the main conceptual ambiguity in multiresonator quantum memory. The architecture is not limited to one special comb, but neither can a finite passive device be exactly perfect on a continuous band. The correct statement is:

> A multiresonator memory is a universal passive light–matter interface to the extent that its positive-real spectral admittance approximates the ideal matched admittance on the chosen signal space. The exact worst-case write error is the L^∞ norm of the prompt reflection on that signal space.

This converts earlier conditions into a single hierarchy and adds an operational storage criterion. The Bragg condition is a comb-specific zero-reflection condition. The common-resonator impedance condition is $\Sigma(0) = (\kappa - \gamma_c)/2$. Spectral matching is $\Sigma'(0) = -1$. Spectral-topological

Table 16: Nominal versus fabrication-robust eleven-mode designs under independent ±1% parameter errors (Monte-Carlo, 3000 trials).

design	ρ_0 (nominal)	median ρ	95% ρ	worst η
minimax (nominal)	0.0641	0.088	0.141	0.980
fabrication-robust	0.0730	0.077	0.104	0.989

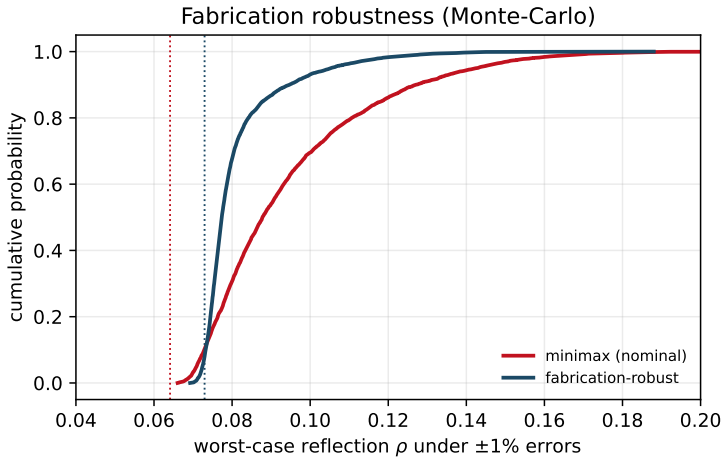

Figure 19: Monte-Carlo distribution of the worst-case reflection ρ under independent ±1% fabrication errors. The fabrication-robust design (blue) has a much tighter tail than the nominal minimax design (red); dotted lines mark the two nominal values.

optimization is finite-pole placement to reduce $N(s)$ over a band. Atomic ensembles and precreated macroscopic coherence improve the design space by adding controllable positive-real terms $\Phi_m(s)$ and programmable rephasing maps that modify absorption, dispersion and retrieval [17].

The remaining open work is now sharply defined. It is not to guess another protocol, but to solve constrained positive-real approximation under fabrication constraints and decoherence constraints. The most important mathematical problems are:

1. closed-form minimax solutions for general N, extending the analytic single-mode optimum $\rho_1 = (\sqrt{2}-1)^2$ and the certified series $N \leq 19$ obtained here;

2. Bode–Fano-type integral bounds specialized to the MR-QM self-energy class;

3. a rigorous proof of Conjecture 1 (the root-exponential rate), e.g. via a Gonchar–Rakhmanov–Stahl analysis of the positive-real Chebyshev problem, yielding a closed-form N-dependent lower bound through the identity (174) to complement the equioscillation and convex certificates established here;

4. non-Markovian and time-dependent extensions that evade finite passive matching bounds for short pulses;

5. full quantum-noise analysis beyond the weak-excitation linear regime;

6. sharp multiport Bode–Fano log-integral bounds, beyond the singular-value capacity floor of Proposition 5;

7. bounded-amplitude dynamic synthesis for finite alphabets, including the exact control penalty imposed by regularized leading tails;

8. protocol-specific network-level standards connecting the Gram/noise/diamond-distance certificate to quantum-interconnect rate and repeater scheduling metrics;

9. passivity-preserving vector fitting with certified Hilbert-transform phase closure and uncertainty budgets for cryogenic microwave and integrated rare-earth experiments.

20 Conclusion

Multiresonator quantum memories can be formulated as passive spectral-admittance synthesizers equipped with controlled storage and retrieval maps. In this formulation the self-energy Σ is positive real, the coherent prompt reflection is its Cayley transform, and the write efficiency is exactly the spectral reflection defect. The same statement extends to vector interfaces by replacing the scalar reflection coefficient with the largest singular value of the prompt scattering matrix.

The theory gives both limitations and constructive design principles. A finite passive time-independent one-port memory cannot be exactly reflectionless on a nonzero continuous band, and the Bode–Fano area law bounds the total logarithmic matching resource. Finite devices are therefore not exact continuous-band universal interfaces; they are controlled approximants whose worst-case error is the minimax reflection norm. Conversely, once the target signal space is finite dimensional or the coupling can be varied in time, exact storage is possible with the appropriate storage dimension and calibrated controls.

The main practical consequence is a certification protocol. A complete MR-QM claim should specify the positive-real admittance or prompt scattering matrix, the controlled-storage dilation, the target signal space, the reflection or singular-value norm, the Bode–Fano area utilization, complex-response uncertainty margins, robustness margins, noise occupancies, and the reciprocal readout map. These data determine the ideal weak-signal memory channel and make different resonator, atomic-ensemble, integrated-photonic and dynamically controlled implementations directly comparable.

The synthesis side of this frontier is now substantially closed. A certified minimax family for $N \le 19$ drives the worst-case reflection geometrically toward the Bode–Fano floor $e^{-\pi}$; each design is shown to be globally optimal by three concordant certificates (equioscillation, the convex weight-optimum, and an independent global search), the optimum is proven minimum-phase and area-saturating, and the residual gap to the floor is identified with a single out-of-band log-area. The abstract self-energy is made buildable through an explicit miniresonator recipe, and a fabrication-robust synthesis trades a fraction of a percent of nominal efficiency for a markedly tighter tolerance to parameter errors. What remains is genuinely mathematical and experimental: a rigorous closed-form N-dependent lower bound to match the equioscillation certificates analytically, and the cryogenic realization of the certified robust geometries. The fixed-pole convex theorem isolates the already-certifiable part; the closed-form global bound is the natural next target.

A Matrix self-energy and Schur complement

For a general passive auxiliary resonator network with mode vector $\boldsymbol{b}$,

$$\dot{a} = -\frac{\kappa + \gamma_c}{2} a - \mathrm{i}\boldsymbol{g}^\dagger \boldsymbol{b} + \sqrt{\kappa} A_{\mathrm{in}}, \tag{177}$$

$$\dot{\boldsymbol{b}} = -(A_b + \Phi(s))\boldsymbol{b} - \mathrm{i}\boldsymbol{g}\, a, \tag{178}$$

where $A_b = \Gamma_b/2 + \mathrm{i}\Omega_b$ has positive semidefinite Hermitian part. Eliminating $\boldsymbol{b}$ gives

$$\Sigma(s) = \boldsymbol{g}^\dagger \left(sI + A_b + \Phi(s)\right)^{-1} \boldsymbol{g}. \tag{179}$$

For $\operatorname{Re} s > 0$ the matrix $sI + A_b + \Phi(s)$ is accretive. Its inverse is also accretive on the range relevant to the Schur complement, giving $\operatorname{Re} \Sigma(s) \geq 0$. This is the matrix form of the positive-real lemma.

B Bound from local matching

Suppose $N(s)$ has a zero of order $p+1$ at $s_0 = \mathrm{i}\omega_0$ and $|D(s)| \geq d_0 > 0$ on $|s - s_0| \leq B$. Cauchy's estimate gives

$$|r(s)| \leq \frac{1}{d_0} \frac{\sup_{|\zeta - s_0| = \rho} |N(\zeta)|}{\rho^{p+1}} |s - s_0|^{p+1}, \qquad |s - s_0| < \rho. \tag{180}$$

Thus a pth-order flat match gives write-error scaling

$$1 - \eta_{\mathrm{w}}^{\min} = O(B^{2p+2}) \tag{181}$$

for sufficiently narrow bands, provided the denominator remains bounded away from zero. This is the rigorous meaning of spectral-dispersion cancellation.

C Finite-dimensional exact storage

Let $\mathcal{S}$ be a K-dimensional subspace spanned by orthonormal spectra f_j. For a stationary one-port device, perfect write on $\mathcal{S}$ requires $Rf_j = 0$ for all j, where R is multiplication by $r(\omega)$. Therefore a nonzero rational r cannot perfectly write any ordinary L^2 pulse mode whose spectral support has positive measure. The exact finite-dimensional stationary statement is an interpolation statement only for idealized distributions:

$$r(\mathrm{i}\omega_j) = 0, \qquad j = 1, \ldots, K, \tag{182}$$

where the f_j are monochromatic frequency-bin limits concentrated at the points ω_j. A rational positive-real self-energy with a feasible positive-real Pick matrix can satisfy these interpolation constraints, but this gives exact delay/absorption for singular frequency bins, not exact capture of normalizable temporal wavepackets. For genuine finite alphabets of temporal modes, exact storage requires time-dependent coupling or an infinite/continuum resource; the constructive dynamic result is Theorem 13.

D Regularized finite-alphabet dynamic capture

For Theorem 13, the accumulated Gram matrix $S(t)$ is singular in the far leading tail because no information about the full alphabet has yet arrived. A deterministic regularization fixes a start time t_0 and a small positive seed matrix $S_0 = \epsilon I_K$. The control uses

$$S_{t_0}(t) = S_0 + \int_{t_0}^{t} \boldsymbol{f}(s) \boldsymbol{f}(s)^{\dagger} \, \mathrm{d}s \tag{183}$$

in place of $S(t)$. The uncaptured probability is bounded by

$$\epsilon_{\mathrm{tail}} = \operatorname{Tr} \int_{-\infty}^{t_0} \boldsymbol{f}(s) \boldsymbol{f}(s)^{\dagger} \, \mathrm{d}s \tag{184}$$

for an incoherent alphabet average, and by the largest eigenvalue of the same omitted Gram matrix for the worst coherent superposition. This gives a finite-amplitude control waveform and an explicit approximation certificate.

E Regularized dynamic-capture schedules

The exact amplitude law $\kappa(t) = |f(t)|^2/E(t)$, supplemented by the phase law $\Delta(t) = -\mathrm{d}\arg f(t)/\mathrm{d}t$ or by equivalent complex coupling control, can diverge in the far leading tail of a pulse because both numerator and denominator are small. This is not a physical singularity of the memory problem; it is a consequence of asking for zero reflection of an infinitely long tail with zero initial stored amplitude. A practical certificate fixes a leading cutoff t_0 with

$$E(t_0) = \epsilon_{\mathrm{tail}}.$$

The memory is initialized with seed energy ϵ_{tail} or, equivalently, the leading tail is discarded. The remaining pulse is captured with

$$\kappa_{t_0}(t) = \frac{|f(t)|^2}{\epsilon_{\mathrm{tail}} + \int_{t_0}^{t} |f(s)|^2\,\mathrm{d}s}, \qquad t \geq t_0,$$

and the unavoidable loss is at most ϵ_{tail}. This regularized schedule is the dynamic analogue of quoting a finite-band reflection certificate: the approximation error is explicit and controllable.

F Noise calibration from measured port occupations

For an experimentally identified scattering matrix, the coherent storage certificate should be supplemented by a normally ordered noise certificate. If the uncontrolled ports q have frequency-dependent thermal occupations $\bar{n}_q(\omega)$ and transfer amplitudes $\ell_q(\mathrm{i}\omega)$ into the output mode, the added output noise for a normalized spectrum f is

$$n_{\mathrm{add}}[f] = \int_{\mathcal{B}} \sum_q |\ell_q(\mathrm{i}\omega)|^2 \bar{n}_q(\omega) |f(\omega)|^2\,\mathrm{d}\omega. \tag{185}$$

For a finite alphabet f_j, the added-noise matrix is

$$(N_{\mathrm{add}})_{ij} = \int_{\mathcal{B}} \sum_q |\ell_q(\mathrm{i}\omega)|^2 \bar{n}_q(\omega) f_i^*(\omega) f_j(\omega)\,\mathrm{d}\omega. \tag{186}$$

This matrix is the noise analogue of the Gram certificate. In optical rare-earth implementations it is often negligible; in microwave or mechanical implementations it can be the decisive quantity unless the uncontrolled ports are cooled or converted into controlled storage ports.

G From parameter tolerances to a self-energy error bound

For the finite positive-real model

$$\Sigma(s) = \sum_n \frac{w_n}{s + \Gamma_n + \mathrm{i}\nu_n}, \tag{187}$$

a deterministic parameter box can be converted to the self-energy error used in Theorem 24. If

$$|\delta w_n| \leq \eta_n^w, \qquad |\delta\Gamma_n + \mathrm{i}\delta\nu_n| \leq \eta_n^p,$$

and $\eta_n^p < \Gamma_n$, then on the imaginary axis

$$|\delta\Sigma(\mathrm{i}\omega)| \leq \sum_n \frac{\eta_n^w}{\Gamma_n} + \sum_n \frac{(w_n + \eta_n^w)\eta_n^p}{\Gamma_n(\Gamma_n - \eta_n^p)}. \tag{188}$$

Indeed,

$$\left| \frac{w_n + \delta w_n}{s + \Gamma_n + \delta\Gamma_n + \mathrm{i}(\nu_n + \delta\nu_n)} - \frac{w_n}{s + \Gamma_n + \mathrm{i}\nu_n} \right| \leq \frac{|\delta w_n|}{\Gamma_n} + \frac{(w_n + |\delta w_n|)|\delta\Gamma_n + \mathrm{i}\delta\nu_n|}{\Gamma_n(\Gamma_n - |\delta\Gamma_n + \mathrm{i}\delta\nu_n|)}.$$

Combining Eq. (188) with Eq. (145) gives a fully deterministic fabrication-tolerance certificate.

H Bode–Fano diagnostic for measured reflection data

Given a measured reflection spectrum over a broad window, the integral

$$A_\Omega = \int_{-\Omega}^{\Omega} \log |r(\mathrm{i}\omega)|^{-1} \, \mathrm{d}\omega \tag{189}$$

is a lower estimate of the Bode–Fano area. For a passive one-port memory with external coupling κ, consistency requires $A_\Omega \le \pi\kappa$ for every Ω, up to calibration error and additional external ports. If a fit claims both a very small reflection over a broad interval and a fixed one-port coupling κ but violates this inequality, the fit cannot be a passive one-port MR-QM. This diagnostic is independent of microscopic modeling and uses only the measured coherent reflection coefficient.

I Vector-port measurement diagnostic

For a measured vector-port interface the scalar inverse-Schur test is replaced by a contractivity test. The prompt scattering matrix must obey

$$R(\mathrm{i}\omega)^\dagger R(\mathrm{i}\omega) \preceq I \tag{190}$$

up to calibration error if the retained model contains all prompt output channels and all irreversible gain has been excluded. A finite-band memory certificate is then

$$\rho_{\mathrm{vec}} = \operatorname*{ess\,sup}_{\omega\in\mathcal{B}} \sigma_{\max}(R(\mathrm{i}\omega)) \,, \qquad \eta_{\mathrm{w}}^{\min} = 1 - \rho_{\mathrm{vec}}^2. \tag{191}$$

If the measured R is noncontractive on a frequency interval, either the calibration is wrong, the model omits an input channel, or an active element contributes gain. In the latter case the passive Bode–Fano and positive-real certificates no longer apply without an added noise analysis.

J Inverse Schur map and realizability test

The normalized inverse map used in Theorem 8 is

$$\Sigma_r(s) = \frac{1 + r(s)}{1 - r(s)} - s. \tag{192}$$

For measured complex data this gives a direct passive-realizability diagnostic. The fitted rational function must have no unstable poles, the inverse admittance must be positive real, and the real and imaginary parts must obey the Hilbert-transform constraints imposed by analyticity. A magnitude-only reflection spectrum can pass the write-efficiency bound while failing this stronger memory-grade test, because all-pass factors leave $|r|$ unchanged but alter the causal phase of the write–read channel.

K Storage-port transfer amplitudes

For the normalized one-port model with $\kappa = 2$ and self-energy

$$\Sigma(s) = \sum_n \frac{w_n}{s + \Gamma_n + \mathrm{i}\nu_n}, \tag{193}$$

the controlled-storage dilation gives

$$a(s) = \frac{-\sqrt{2}}{s + 1 + \Sigma(s)} f_{\mathrm{in}}(s), \tag{194}$$

with the sign convention of Eqs. (158)–(160). The transfer amplitude into the nth storage port is therefore

$$t_n(s) = \frac{\mathrm{i}\,2\sqrt{\Gamma_n w_n}}{(s + \Gamma_n + \mathrm{i}\nu_n)\,[s + 1 + \Sigma(s)]}. \tag{195}$$

For symmetric detuned pairs both members are included in the sum. Direct substitution into

$$r(s) = \frac{s - 1 + \Sigma(s)}{s + 1 + \Sigma(s)} \tag{196}$$

verifies on $s = \mathrm{i}\omega$ that

$$|r(\mathrm{i}\omega)|^2 + \sum_n |t_n(\mathrm{i}\omega)|^2 = 1, \tag{197}$$

which is the frequency-domain form of the energy balance used in the numerical ODE checks.

References

[1] A. I. Lvovsky, B. C. Sanders, and W. Tittel, "Optical quantum memory," *Nature Photonics* **3**, 706–714 (2009).

[2] K. Heshami, D. G. England, P. C. Humphreys, P. J. Bustard, V. M. Acosta, J. Nunn, and B. J. Sussman, "Quantum memories: emerging applications and recent advances," *Journal of Modern Optics* **63**, 2005–2028 (2016).

[3] Y. Lei, H. An, Z. Li, C. Simon, and M. Hosseini, "Quantum optical memory for entanglement distribution," *Optica* **10**, 1511–1528 (2023).

[4] M. Afzelius, C. Simon, H. de Riedmatten, and N. Gisin, "Multimode quantum memory based on atomic frequency combs," *Physical Review A* **79**, 052329 (2009).

[5] M. Afzelius and C. Simon, "Impedance-matched cavity quantum memory," *Physical Review A* **82**, 022310 (2010).

[6] S. A. Moiseev, S. N. Andrianov, and F. F. Gubaidullin, "Efficient multimode quantum memory based on photon echo in an optimal QED cavity," *Physical Review A* **82**, 022311 (2010).

[7] S. A. Moiseev, "Multiresonator quantum memory," *Physical Review A* **95**, 012338 (2017).

[8] S. A. Moiseev, K. I. Gerasimov, R. R. Latypov, N. S. Perminov, K. V. Petrovnin, and O. N. Sherstyukov, "Broadband multiresonator quantum memory-interface," *Scientific Reports* **8**, 3982 (2018).

[9] K. V. Petrovnin, N. S. Perminov, O. N. Sherstyukov, and S. A. Moiseev, "Microwave quantum memory on a controlled frequency comb," *Quantum Electronics* **48**, 898–901 (2018).

[10] N. S. Perminov, D. Yu. Tarankova, and S. A. Moiseev, "Superefficient cascade multiresonator quantum memory," *Laser Physics Letters* **15**, 125203 (2018).

[11] N. S. Perminov and S. A. Moiseev, "Spectral-topological superefficient quantum memory," *Scientific Reports* **9**, 1568 (2019).

[12] Z. Bao, Z. Wang, Y. Wu, Y. Li, C. Ma, Y. Song, H. Zhang, and L. Duan, "On-demand storage and retrieval of microwave photons using a superconducting multiresonator quantum memory," *Physical Review Letters* **127**, 010503 (2021).

[13] N. S. Perminov and S. A. Moiseev, "Integrated multiresonator quantum memory," *Entropy* **25**, 623 (2023).

[14] A. R. Matanin, N. S. Smirnov, A. I. Ivanov, V. I. Polozov, D. A. Moskaleva, E. I. Malevannaya, M. V. Androshuk, Y. A. Agafonova, D. E. Shirokov, A. V. Andriyash, and I. A. Rodionov, "Superconducting integrated on-demand quantum memory with microwave pulse preservation," *Physical Review Letters* **136**, 060807 (2026), doi:10.1103/m9qc-ppk3.

[15] H. An, Z. Li, and M. Hosseini, "Preparation-free resonator array atomic memory for on-chip quantum storage," *APL Quantum* **2**, 026134 (2025).

[16] S. A. Moiseev, "Multiresonator quantum memory with atomic ensembles," *Physical Review A* **113**, 022419 (2026), doi:10.1103/zln6-jzvm; arXiv:2507.04865 [quant-ph].

[17] S. A. Moiseev, K. I. Gerasimov, M. M. Minnegaliev, and E. S. Moiseev, "Optical quantum memory on macroscopic coherence," *Physical Review Letters* **134**, 070803 (2025).

[18] R.-R. Meng, P.-X. Liu, X. Liu, T.-X. Zhu, P.-J. Liang, C. Zhang, Z.-Y. Tang, H.-Z. Zhang, J.-M. Cui, M. Jin, Z.-Q. Zhou, C.-F. Li, and G.-C. Guo, "Efficient integrated quantum memory for light," *Nature Photonics* **20**, 437–443 (2026), doi:10.1038/s41566-026-01845-y.

[19] H.-X. Luo, C. Li, J.-L. Ren, Y. Yuan, Y.-L. Wen, J.-F. Li, Y.-F. Wang, S.-C. Zhang, H. Yan, and S.-L. Zhu, "A high-performance quantum memory for quantum interconnects," arXiv:2603.01156 [quant-ph] (2026).

[20] H. W. Bode, *Network Analysis and Feedback Amplifier Design* (Van Nostrand, New York, 1945).

[21] R. M. Fano, "Theoretical limitations on the broadband matching of arbitrary impedances," *Journal of the Franklin Institute* **249**, 57–83 and 139–154 (1950).

[22] L. Greggio, T. Lorriaux, A. Petrescu, M. Mirrahimi, and A. Bienfait, "Optimal absorption and emission of itinerant fields into a spin-ensemble memory," *Physical Review A*, accepted (2026), doi:10.1103/6xjr-tflh; arXiv:2506.06107v3 [quant-ph].

[23] J. Dilley, P. Nisbet-Jones, B. W. Shore, and A. Kuhn, "Single-photon absorption in coupled atom-cavity systems," *Physical Review A* **85**, 023834 (2012).

[24] A. Shlivinski and Y. Hadad, "Beyond the Bode-Fano bound: Wideband impedance matching for short pulses," *Physical Review Letters* **121**, 204301 (2018).

[25] C. W. Gardiner and M. J. Collett, "Input and output in damped quantum systems: Quantum stochastic differential equations and the master equation," *Physical Review A* **31**, 3761–3774 (1985).

[26] J. E. Gough and G. Zhang, "On realization theory of quantum linear systems," *Automatica* **59**, 139–151 (2015).

[27] H. I. Nurdin, "The transfer function of generic linear quantum stochastic systems has a pure cascade realization," *Automatica* **69**, 324–333 (2016).

[28] R. M. Fano, "Theoretical limitations on the broadband matching of arbitrary impedances," Research Laboratory of Electronics, MIT Technical Report No. 41 (1948).

[29] G. L. Matthaei, L. Young, and E. M. T. Jones, *Microwave Filters, Impedance-Matching Networks, and Coupling Structures* (McGraw–Hill, New York, 1964).

[30] A. R. Matanin, K. I. Gerasimov, E. S. Moiseev, N. S. Smirnov, A. I. Ivanov, E. I. Malevannaya, V. I. Polozov, E. V. Zikiy, A. A. Samoilov, I. A. Rodionov, and S. A. Moiseev, "Toward Highly Efficient Multimode Superconducting Quantum Memory," *Phys. Rev. Applied* **19**, 034011 (2023), doi:10.1103/PhysRevApplied.19.034011.

[31] A. V. Gorshkov, A. André, M. D. Lukin, and A. S. Sørensen, "Photon storage in Λ-type optically dense atomic media. II. Free-space model," *Phys. Rev. A* **76**, 033805 (2007); see also *Phys. Rev. Lett.* **98**, 123601 (2007), doi:10.1103/PhysRevA.76.033805.

[32] X. Nie and B. M. Hochwald, "Bandwidth Analysis of Multiport Radio-Frequency Systems," *IEEE Trans. Antennas Propag.* **65**(3), 1081–1092 (2017), doi:10.1109/TAP.2017.2653252; arXiv:1509.02152.

[33] Y. Zhou *et al.*, "Efficient on-chip platform for coherent light–matter coupling using bound states in the continuum," *Sci. Adv.* **11**, eadu0976 (2025), doi:10.1126/sciadv.adu0976.